

**Conformational Analysis of 2-Butyne-1, 4-diol:  
A Matrix Isolation FTIR and *Ab-Initio* Study**

**Himanshi Singh**

MS14084

*BS-MS dual degree in science*



Indian Institute of Science Education and Research Mohali

April 2019



## **Certificate of Examination**

This is to certify that the dissertation titled “Conformational Analysis of 2-Butyne-1,4-diol: A Matrix Isolation FTIR and *Ab-Initio* Study” submitted by Ms. Himanshi Singh (Reg. No. MS14084) for the partial fulfillment of BS-MS dual degree program of the Institute, has been examined by the thesis committee duly appointed by the Institute. The committee finds the work done by the candidate satisfactory and recommends that the report be accepted.

Dr. S. Venkataramani

Dr. P. Balanarayan

Prof. K. S. Viswanathan

Dated: April, 26, 2019



## **Declaration**

The work presented in this dissertation has been carried out by me under the guidance of Prof. K. S. Viswanathan at the Indian Institute of Science Education and Research Mohali.

This work has not been submitted in part or in full for a degree, a diploma, or a fellowship to any other university or institute. Whenever contributions of others are involved, every effort is made to indicate this clearly, with due acknowledgment of collaborative research and discussions. This thesis is a bonafide record of original work done by me and all sources listed within have been detailed in the bibliography.

Himanshi Singh

MS14084

Dated: April 26, 2019

In my capacity as the supervisor of the candidate's project work, I certify that the above statements by the candidate are true to the best of my knowledge.

Prof. K. S. Viswanathan

(Supervisor)



## **Acknowledgments**

Firstly, I would like to express my sincere gratitude and acknowledgment to my thesis supervisor Prof. K.S. Viswanathan for his constant support and guidance over the past years. I thank him for being my mentor, teacher, his valuable discussions have shaped me not only as a researcher but, also as a person.

I also thank my thesis committee members Dr. S. Venkataramani and Dr. P. Balanarayan for their valuable discussions and suggestions. I want to thank current Director Prof. Arvind, former Director Prof. D.P. Sarkar, and founding director Prof. N. Sathyamurthy, for supporting me with all the facilities at IISER-Mohali. I gratefully acknowledge DST for providing INSPIRE fellowship to pursue my BS-MS degree.

A sincere thanks to my lab members Pankaj, Jai, Shivangi, Dipali especially to Jyoti for being an amazing mentor. They provided a learning environment in the lab and provided their useful suggestions regarding the work and in understanding the working of MT-FTIR set-up. A special thanks to POC lab members: Mayank, Chitranjan for their help over this past two semesters.

I owe special thanks to my friends Meenakshi, Swati, and Chatha floor for making my hostel life fun. A special mention to my Vehlas: Navnoor, Jorawar, Ajeet. All those late night writing sessions, gossiping are the beautiful moments which I will cherish all my life. I owe them a lot for always tolerating me and helping me whenever I needed their support.

Shubham, Thank You!

Most importantly, I would like to thank my parents, Mr. Madan Lal and Mrs. Meena Kumari for their continuous encouragement in this five-year long journey. I also thank my siblings, Satyam, and Shivam for their constant support. Their roles have been instrumental in the development and shaping of my academic career.



# Table of Contents

<b>List of Figures</b> .....	iv
<b>List of Tables</b> .....	vi
<b>List of Abbreviations</b> .....	viii
<b>Abstract</b> .....	x
<b>1. Introduction</b> .....	1
1.1 Hydrogen Bonding .....	1
1.2 Definition of Hydrogen bond .....	2
1.3 Methods to Study Weak Hydrogen Bonds .....	3
1.3.1 Spectroscopic methods .....	3
1.3.2 Crystallography .....	3
1.3.3 Computational studies .....	3
1.4 Motivation .....	4
<b>2. Experimental and Computational Procedures</b> .....	7
2.1 What is Matrix –Isolation?.....	7
2.2 Nature of Matrix.....	8
2.3 Solvation Effects of Matrix.....	8
2.3.1 Matrix effects.....	8
2.3.3 Aggregation .....	11
2.3.5 Rotation of guest molecule in matrix cage .....	12
2.5 Advantages of Matrix Isolation and its Limitations.....	12
2.6 Matrix Isolation Infrared Setup .....	13
2.7 Computational Methods and Procedures .....	21
2.7.1 Level of theory.....	21
2.7.2 Basis sets.....	22
2.7.3 Geometry optimization and frequency calculation.....	24
2.7.4 Energy calculations.....	25
2.7.4 Atom in molecules analysis .....	26
2.7.4 Localized molecular orbital energy decomposition analysis.....	27

2.7.5 Natural bond orbital analysis .....	28
<b>3. Results and Discussion</b> .....	31
<b>3.1 2-Butyne-1,4-diol</b> .....	31
3.1.1 Computational results .....	31
3.1.2 Experimental results .....	37
3.2 Interaction studies of 2-Butyne-1, 4-diol –Water complexes .....	41
<b>4. Conclusion</b> .....	49
4.1 Influence of acetylenic $\pi$ -cloud .....	49
4.2 Future Scope.....	54
<b>Bibliography</b> .....	55
<b>Appendix</b> .....	59

## List of Figures

<b>Fig.</b>	<b>Caption</b>	<b>Page No.</b>
1.1	Multifunctional molecular system under investigation	5
2.1	Cartoon depicting the matrix isolation technique	7
2.2:	Plot depicting the dependence of U, U' and U'' on the matrix cage	10
2.3	Schematic of closed cycle cryocooler	14
2.4	Cryostat and its associated units	15
2.5(a)	Rotary vane pump	16
2.5(b)	Schematic of oil diffusion pump	16
2.6(a)	Pirani gauge	17
2.6(b)	Penning gauge	17
2.7	Sample introduction assembly	18
2.8	Schematic diagram of FTIR spectrophotometer	19
2.9	Home-built matrix isolation set-up at IISER	20
2.10	Optimization based on energy	24
3.1	2-Butyne-1,4-diol	31
3.2	Nomenclature for the notation of 2-Butyne-1,4-diol conformations	32
3.3	Conformations of 2-Butyne-1,4-diol	32
3.4	AIM analysis of 2-Butynediol	33

<b>3.5</b>	Correlation diagram showing the energy (in kcal/mol) of gauche and trans conformer of BYD, at M06-2X/aug-cc-pVDZ when orbital interactions were systematically deleted.	36
<b>3.6</b>	Glass bulb containing sample	37
<b>3.7</b>	Schematic of the setup used for matrix isolation FTIR experiments	38
<b>3.8</b>	A comparison between computed and experimental spectrum for 2-Butyne-1, 4-diol in N <sub>2</sub> matrix 12K. A: Experimental Spectrum; B, C and D: Computed spectrum of BYDA, BYDB and BYDC respectively; E: Sum of the computed spectrum for all the three conformers BYDA, BYDB and BYDC.	39
<b>3.9</b>	Optimized structures of BYD-A complexes at the HF/3-21G level of theory. Uncorrected energies in Ha	41
<b>3.10</b>	Optimized structures of BYDA-W_III and complexes of water with higher energy conformers of BYD at M06-2X/aug-cc-pVDZ level. Hydrogen-bonded distances have been shown as dotted lines with bond distances in Å units. Change in the linearity of C-C-C-C backbone is given in %	42
<b>3.11</b>	Correlation diagram to show the relative locations of BYD-W complexes on the energy axis. The difference in energy between the monomer asymptote and the complexes corresponds to uncorrected interaction energy (Ha) at M06-2X/aug-cc-pVDZ level. The plotted energy levels are to scale on the energy axis.	43
<b>3.12</b>	AIM analysis of BYD-W complexes	44
<b>4.1</b>	Ethylene Glycol compared with 2-butynediol	50
<b>4.2</b>	Comparison of propargyl alcohol and 2-butynediol	53

## List of Tables

<b>Table No.</b>	<b>Caption</b>	<b>Page No.</b>
2.1	Level of theories	21
2.2	Basis sets	23
3.1	Relative energy ordering	33
3.2	NBO analysis for BYDA,BYDB, BYDC and BYDF conformations	34
3.3	Assignment of features for BYDA in N <sub>2</sub> matrix. Computed at MP2/aug-cc-pVDZ; scaled using a factor 0.96, 0.98, 0.99 for OH stretch, OH bent and CO stretch respectively.	40
3.4	Interaction energies for 2-butyne-1,4-diol	43
3.5	AIM analysis of BYDA-W_III,BYDD-W,BYDE-W,BYDF-W and BYDF-W' complexes	45
3.6	NBO analysis of BYDA-W_III, BYDD-W, BYDE-W, BYDF-W and BYDF-W' complexes	46
4.1	NBO analysis of ethylene glycol,EGI(tGg') and 2-butyne-1,4-diol, BYDD(tGg <sup>-</sup> )	51
4.2	NBO analysis of ethylene glycol, EGVII(gGg) and 2-butyne-1,4-diol, BYDB(gGg <sup>-</sup> )	52



## List of Abbreviations

<b>IR</b>	Infrared
<b>UV</b>	Ultraviolet
<b>NMR</b>	Nuclear Magnetic Resonance
<b>BYD</b>	2-Butyne 1,4-diol
<b>PA</b>	Propargyl alcohol
<b>EG</b>	Ethylene glycol
<b>SP</b>	Stationary Point
<b>Elec</b>	Electrostatic
<b>Rep</b>	Repulsive
<b>Dis</b>	Dispersive
<b>Pol</b>	Polarization
<b>Ind</b>	Inductive
<b>GM</b>	Gifford-McMahon
<b>KBr</b>	Potassium Bromide
<b>HF</b>	Hartree-Fock
<b>DFT</b>	Density Functional Theory
<b>B3LYP</b>	3-parameters used in the Beck-Lee-Yang Parr functional
<b>M06</b>	Minnesota functional
<b>MP2</b>	Møller- Plesset 2 Perturbation theory
<b>ZPCE</b>	Zero Point Corrected Energy
<b>BSSE</b>	Basis Set Superposition Error
<b>FWHM</b>	Full Width at Half Maximum
<b>AIM</b>	Atom-In-Molecules Analysis
<b>CP</b>	Critical Point
<b>NBO</b>	Natural Bond Orbital Analysis



## Abstract

The work presents, for the first time, the matrix isolation infrared and *ab initio* studies on the molecular conformations of 2-butyne-1, 4-diol. It is found that when the acetylenic moiety ( $-\text{C}\equiv\text{C}-\text{H}$ ) in propargyl alcohol is replaced by a  $\text{CH}_2\text{OH}$  group, it gives rise to many different conformations of ethylene glycol, which are facilitated by strong intramolecular  $\text{O}-\text{H}\cdots\text{O}$  hydrogen bonded interactions. Similarly, when the acidic hydrogen in propargyl alcohol is replaced by a  $\text{CH}_2\text{OH}$  group, several conformations arise for 2-butyne-1, 4-diol. Thus, these molecules, propargyl alcohol, ethylene glycol and 2-butyne-1,4-diol provide an interesting case to study the effect of an acetylenic  $\pi$  cloud between the two  $-\text{OH}$  groups on the conformations, which was absent in ethylene glycol. Starting from only two stable conformers in propargyl alcohol and ten stable conformers in ethylene glycol, we have computed six stable conformers of 2-butyne-1,4-diol in this work at M06-2X and MP2 methods employing 6-311++G\*\* and aug-cc-pVDZ basis sets. Our experiments together with computations revealed the presence of three most stable conformers in the  $\text{N}_2$  matrix. AIM and NBO analysis have been performed to understand the nature of interactions in the conformers. Vicinal orbital interactions are found to play a deciding role in its conformational preference.

Competitive hydrogen bonding because of the presence of multiple bonding sites in 2-butyne-1, 4-diol is another aspect which we have explored from our computational studies on its hydrogen-bonded complexes with water.



# Chapter 1

## Introduction

Non-covalent interactions are extensive and form an essential part of chemistry, physics, and biology. These weak interactions determine the structure of biomolecules such as DNA and also drives the folding of proteins. Thus, an in-depth understanding of these weak interactions may lead to the design of drugs and functional materials. These non-covalent interactions have a broad range of classification depending on nature, origin, and strength. Hydrogen bonding is the most versatile non-covalent interaction that has been described in the next section.

### 1.1 Hydrogen Bonding

Hydrogen bonds are the most critical form of non-covalent interactions that govern several biological and chemical processes. A pervasive example of a hydrogen bond is found in between water molecules which is responsible for the unique solvent properties of water. Right from holding the strands of DNA together to the protein folding, these chemical interactions govern life form and functions. Hydrogen bonds also play a dominant role in supramolecular chemistry<sup>1</sup> for designing molecules with desired properties. <sup>2</sup>Thus, there is great significance of Hydrogen bonding in our life, thereby making the study of these interactions important.<sup>3</sup>The first observation of Hydrogen bond was in the year 1902, and it was termed as “Nebenvalenz” (minor valence). Few more such reports followed it, and in 1912 it was redefined as “weak unions” to describe the properties of trimethylammonium hydroxide in comparison with the tetramethylammonium hydroxide<sup>4</sup>. <sup>5</sup>In 1920, Latimer and Rodebush suggested that ‘a free pair of electrons on one water molecule might be able to exert sufficient force on a hydrogen held by a pair of free electrons on another water molecule to bind the two molecules together’ and that ‘the hydrogen nucleus held between the two octets constitute a *weak bond*’. These terms to Hydrogen bond kept on being redefined until 1939 when <sup>3</sup>Pauling used the term *Hydrogen bond* for the first time and introduced it as an essential principle in chemistry. Pauling described hydrogen bond as an electrostatic interaction which limits the hydrogen bond to be only present when a hydrogen atom is attached to a highly electronegative atom (N, F, and O). In 1960, Pimentel and McClellan addressed the limitation of hydrogen bonding and accounted for the possibility of hydrogen bonding interactions with the groups such as C-H, P-H, Si-H and of  $\pi$ -acceptor and many other groups.<sup>6</sup>

## 1.2 Definition of Hydrogen bond

An accurate definition of the hydrogen bond remained ambiguous for a long time. But, to account for the recent experimental and theoretical findings for hydrogen bonding interactions, International Union of Applied and Pure Chemistry formed a committee of eminent scientists that proposed a modern definition of hydrogen bond <sup>7</sup>in the year 2011 as follows:

*“The hydrogen bond is an attractive interaction between a hydrogen atom from a molecular fragment X-H in which X is more electronegative than H, and an atom or a group of atoms in the same or different molecule, in which there is evidence of bond formation.”*

This definition broadens the criteria needed to classify an interaction as a Hydrogen bond. A hydrogen bond can be represented as X-H...Y-Z, where X-H acts as hydrogen bond donor and Y can be an atom or an anion, or a fragment or a molecule. A ‘symmetric hydrogen bond’ is formed when X and Y are the same such that the X-H and Y-H distances become equal. The acceptor is an electron-rich region, which can be anything ranging from very electronegative atom to a lone pair or a  $\pi$ -bond pair. The definition accounts for all possible donors and acceptors that can take part in hydrogen bonding, hence also taking into consideration the formation of a weak hydrogen bond where either donor or acceptor or both of them have moderate or low electronegativity.

A hydrogen bond is a strong electrostatic and a partially covalent interaction which is weaker than an ionic or a covalent bond having an energy in a range of -0.5 kcal/mol to -40.0 kcal/mol. <sup>8</sup>There is a particular criterion to distinguish very strong, strong and weak hydrogen bonds that could be based on energy, thermodynamics or functional aspects. One such method is based upon bond energies; the very strong hydrogen bonds have their energies in the range of -15.0 to -40.0 kcal/mol as found in  $[F\cdots H\cdots F]^-$  and  $[N\cdots H\cdots N]^+$ . Strong hydrogen bonds such as  $O-H\cdots O=C$ ,  $O-H\cdots O=C$  have their bond energy in the range of -4.0 to -15.0 kcal/mol. Hydrogen bonds with bond energies in the range of -1.0 to -4.0 kcal/mol are termed as weak hydrogen bonds and involve proton donors such as C-H or S-H acceptors as  $\pi$  systems. These weak hydrogen bond interactions can undergo rearrangements at ambient temperature, in short time spans thus making them important in chemistry and biology<sup>9</sup>. Investigation of these weak interactions is challenging, but these can be studied using various methods.

### **1.3 Methods to Study Weak Hydrogen Bonds**

There are several instrumental and computational techniques to study the weak hydrogen bonds that include spectroscopic methods, diffraction methods, NMR and computational methods.

#### **1.3.1 Spectroscopic methods**

Infrared spectroscopy is a popular method to study different types of hydrogen bonds, both in solid and solution state. The formation of hydrogen bond causes notable changes in the vibrational spectra of the molecules depending upon the strength of the interactions involved between them. These changes are actually the frequency shifts which occur due to the formation of the hydrogen bond. When a hydrogen bond forms in X-H...Y fashion, there is an elongation of X-H bond and weakening of bond due to electron density transfer from proton acceptor to proton donor's sigma antibonding which gets reflected as redshift and increase in intensity. A blue shift and a decrease in intensity are observed when an X-H bond is compressed rather than elongation such hydrogen bonds are termed as improper hydrogen bonds.

Gas phase rotational spectroscopy is also used to investigate hydrogen-bonded adducts that are at a global minimum. These studies allow us to obtain various parameters like dissociation energies, force constants, geometries which otherwise are not possible to obtain with the experiments in the condensed phase.

#### **1.3.2 Crystallography**

Diffraction methods can easily detect weak hydrogen bonds as compared to the spectroscopic techniques. The technique helps to determine the three-dimensional structure of molecules to atomic resolution. X-ray diffraction is an important method in determining the position of hydrogen bonds, where X-rays interact with the electron density of the molecule under consideration. The advances in low-temperature technique coupled with X-ray diffraction have proven to be invaluable. Neutron diffraction serves as a more accurate method in locating the position of hydrogen atoms, where neutrons interact with the nuclei of the atoms.

#### **1.3.3 Computational studies**

Computational studies provide us the information about the geometry of the molecules which when complimented with the experimental results enhances our understanding of hydrogen bonding. Computations provide information on interaction energies and the nature of hydrogen bonding interaction without any complicated effects of the solvent or solid state environment. The

*ab initio* computations help in optimization of different geometries and vibrational frequency calculations ensure that these geometries are indeed minima on the potential energy surface with the positive values for all the frequencies of different normal modes. These computed frequencies are then used to assign the experimental features.

## 1.4 Motivation

It is interesting to study the molecules having multiple hydrogen bonding sites, especially when these sites are equally competitive in terms of weak non-covalent interactions as it allows us to investigate competitive hydrogen bonding. To exemplify how there exists a hydrogen bonding competition among various sites, we present a case study of multifunctional molecules such as propargyl alcohol, ethylene glycol, and 2-butyne-1,4-diol. The structures of these molecules have been provided in Fig 1.1. Propargyl alcohol can act as a proton donor through its acidic hydrogen and the hydroxyl group, and as a proton acceptor through its O atom and the  $\pi$  electron cloud. Thus, when propargyl alcohol is involved in H-bonding, there exists a competition whether it will serve as a proton donor or as a proton acceptor.

*Ab-Initio* studies on propargyl Alcohol report two stable conformations – gauche and trans; however, only the most stable gauche isomer was observed in the matrix isolation infrared experiments<sup>10</sup>. Further, in propargyl alcohol, if the acetylenic moiety ( $-\text{C}\equiv\text{C}-\text{H}$ ) is replaced by a  $\text{CH}_2\text{OH}$  group, many different conformations of ethylene glycol are obtained. As now two OH groups can be either in gauche or trans configuration with the C-C bond, but also the two CO groups can also orient themselves as gauche or trans. In ethylene glycol, the most stable conformers were bound by a weak intramolecular  $\text{O}-\text{H}\cdots\text{O}$  hydrogen bonded interactions which have been justified based on redshift.

We then chose the system, 2-Butyne-1,4-diol or BYD having two hydroxyl groups similar to that in ethylene glycol together with a  $\pi$  electron cloud. Thus, BYD is a molecule obtained on replacing the acidic hydrogen in propargyl alcohol by a  $\text{CH}_2\text{OH}$  group. It is interesting to study the conformations of BYD which could be stabilized by an intramolecular  $\text{O}-\text{H}\cdots\text{O}$  or  $\text{O}-\text{H}\cdots\pi$  hydrogen bonded interaction. Another interesting aspect is the orientation of the two  $-\text{OH}$  groups about the  $\pi$  electron density which can result in the geometry showing atropisomerism similar to biphenyls, thus we wished to explore different conformations of BYD in this work.

Computational studies on ethylene glycol and propargyl alcohol claim the stability of gauche conformers over the trans; the trend is expected to be observed in 2-Butyne-1,4-diol. The stability of gauche conformers in ethylene glycol is dictated by weak intramolecular hydrogen bonding interactions observed through the Natural Bond Orbital (NBO) analysis and the red-shift in the OH stretch region.

Hence, it provides a compelling case to study the influence of acetylenic  $\pi$  cloud on the conformations of the previously studied ethylene glycol system. BYD finds its application<sup>11</sup> in cleansing agents and majorly as a precursor for polyurethanes, vitamin B<sub>6</sub>, alkyd resins, and plasticizers.

The BYD-water system is another system of particular interest from the hydrogen bonding point of view as there exist multiple proton donor and acceptor sites. It is intriguing to understand how the water molecule will orient itself in the proximity of multifunctional groups and in such a scenario, which geometry will constitute the global minimum for BYD-water complex.

In short, the primary motivation of this work is to address the question: What is the influence of acetylenic  $\pi$ -cloud on the conformations of ethylene glycol, which seems to occur as a spacer between the two diols in ethylene glycol. This work, thus, presents a detailed understanding of the conformationally rich species, 2-Butyne-1,4-diol through a Matrix isolation FTIR spectroscopic and the *ab-initio* study. Competitive hydrogen bonding in the 2-Butyne-1,4-diol system is then explored through computations performed on its complexes with a water molecule.

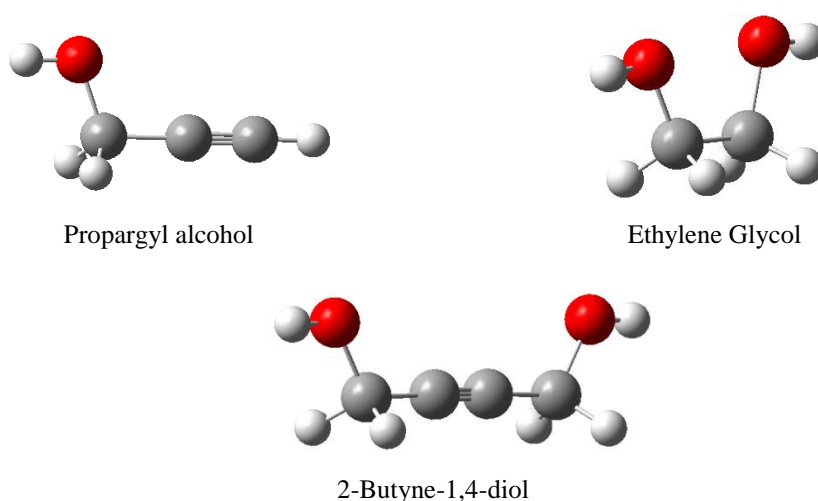


**Fig. 1.1:** Multifunctional molecular system under investigation



## Chapter 2

### Experimental and Computational Procedures

The present section deals with the experimental aspects of matrix isolation infrared spectroscopy that has been used to study the conformations of 2-butyne-1, 4-diol.

#### 2.1 What is Matrix –Isolation?

The term “matrix isolation” was coined by George C. Pimentel<sup>12</sup> together with George Porter<sup>13</sup>. The technique consists of trapping of guest molecules in the host gas, at a very low temperature and to study them using various spectroscopic tools. The typical guest to host ratios used in a range of  $1:10^3$  to  $1:10^5$  diminishes any intermolecular reactions within the guest species and leads to uncongested spectra with smaller linewidths. The low temperatures usually in the range of 4 K to 20 K, prevent the occurring of any processes with activation energy more than a few kJ/mole.

<sup>14</sup>This technique can be used to study unstable molecules with short lifetime such as radicals, carbocations, carbanions, carbenes, reactive intermediates, conformers, etc., and to study different types of weak non-covalent interactions such as H-bonding interactions.<sup>15</sup> The matrix isolation technique is coupled with a variety of spectroscopic probes for experimental detection and analysis of guest species such as FT-IR, UV-Visible<sup>16</sup> and ESR<sup>17</sup> spectroscopy for chemical analysis of isolated species.

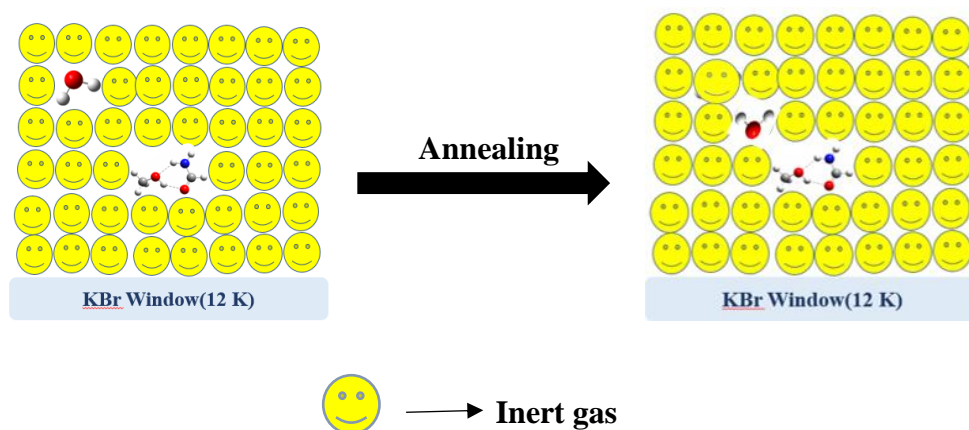


**Fig. 2.3:** Cartoon depicting matrix isolation technique

## 2.2 Nature of Matrix

Matrix host material should be chemically inert like noble gases such as Ne, Ar are the best choices, although in many cases the heavier noble gases, N<sub>2</sub>, CH<sub>4</sub>, H<sub>2</sub> or other inert molecular hosts, may also be used. On the other hand, one can deliberately choose a matrix material that is reactive toward the targeted intermediate, for example, CO or O<sub>2</sub>, to trap carbenes<sup>18</sup> or nitrenes<sup>19</sup>, but that preserves the other advantages over polyatomic solvents.

The two most important criteria for the host species to serve as a matrix are the inertness and transparency in the spectral region of interest. The matrix must cause minimal chemical perturbation to the sample of interest. Matrix should be free from any absorption in the region of interest as that would interfere with the detection of the isolated molecule. The matrix must be chosen as per the experiment requirement, for example, p-H<sub>2</sub> is well suited for the study of Polycyclic Aromatic Hydrocarbons but is unfit for the study of H-bonding interactions<sup>20</sup>.

The cold substrate where the matrix is deposited is usually at a temperature below one-third of the melting point of the host gas prevents diffusion and ensures the uniformity and rigidity of the matrix. Another important factor is the purity; it should be highly pure. The matrix species should not be of a large molecular size which increases the van der Waal forces.

The matrix formed can be considered as a micro-crystalline inert material where diffusion is prohibited or a crystal with the region of defects serving as a trapping site for the molecules of interest. As a result of these defect, the site effects come into play a critical role in the analysis of isolated species. Inert gases such as Ar freezes in FCC lattice while N<sub>2</sub> freezes in HCP lattice<sup>21</sup>. Each atom is surrounded by 12 nearest neighbors. FCC and HCP both occupy 74% of the lattice while 24% remains unoccupied. These closed packed lattices have two possible occupational sites the interstitial site and the substitutional site.

## 2.3 Solvation Effects of Matrix

### 2.3.1 Matrix effects

The interaction of the trapped species with the matrix atoms perturbs the vibrational modes of isolated species which is reflected as shifts in IR frequencies compared with the gas phase data. These frequency shifts in matrix experiments relative to gas phase values arise because of the following interactions:

1) Electrostatic interaction-( $\Delta \nu_{elec}$ )

2) Inductive interaction-( $\Delta \nu_{ind}$ )

3) Long range Dispersion interactions-( $\Delta \nu_{dis}$ )

4) Short range Repulsive interactions-( $\Delta \nu_{rep}$ )

$$\Delta \nu = (\nu_{matrix} - \nu_{gas}) = \Delta \nu_{elec} + \Delta \nu_{ind} + \Delta \nu_{dis} + \Delta \nu_{rep} \dots$$

Where  $\nu_{matrix}$  is the frequency of a given sample in the matrix experiment while  $\nu_{gas}$  is the frequency of the same sample in the isolated gas phase. These shifts are a measure of the strength of the interactions. These  $\Delta \nu_{dis}$ ,  $\Delta \nu_{rep}$  vary as per the choice of host. Usually, for inert gases, dispersive and repulsive interactions dominate.

As discussed before the matrix host gases crystallize in different lattices with different lattice parameters. Hence the environment experienced by the host differs depending on the matrix. Theoretically, it has been shown that tight cages result in blue shifts<sup>22</sup> and loose cages lead to redshifts in the vibrational frequencies of the guest sample. Pimentel and Charles<sup>23</sup> have used Buckingham model<sup>24</sup> to explain the effect of a solvent environment on the vibrational frequency of the guest molecule. The model applied over the inert gas cages reduces the:

$$\Delta \nu = (\nu_{matrix} - \nu_{gas}) = \frac{B_e}{hcw_e} \left[ U'' - 3 \frac{A}{w_e} U' \right]$$

Where,

$$B_e = \frac{h}{8\pi^2 m_r c r_e^2} \text{ is the rotational constant}$$

A=Anharmonicity constant

U=Energy due to solute-solvent interactions

$U' = \left\{ \frac{\partial U}{\partial r_{BC}} \right\}$  and  $U'' = \left\{ \frac{\partial^2 U}{\partial^2 r_{BC}} \right\}$ ,  $r_{BC}$  = equilibrium distance between B and C of the molecule ABC as shown in the Fig 2.2.

$cw_e$  =Harmonic Oscillator frequency

In Fig. 2.2 ABC represents a triatomic molecule trapped inside a matrix cage and the matrix atom 'M' is the nearest neighbor to C.

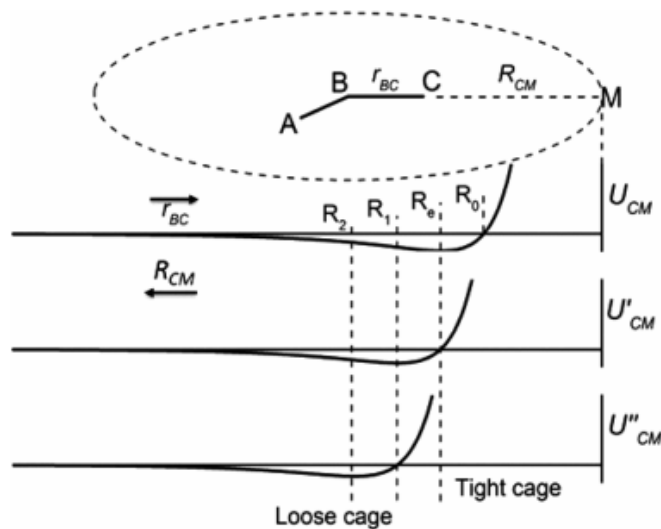


**Fig 2.2:** Plot depicting the dependence of  $U$ ,  $U'$  and  $U''$  on the matrix cage

In a tight cage the distance between atoms C and the M,  $R_{CM}$  is less than  $R_e$  ( $R_{CM} < R_e$ ) which suggests that  $U''$  term in the above equation is positive, that implies a positive value of  $\Delta\nu$  and therefore a blue shift. For a loose cage,  $R_{CM}$  is greater than  $R_e$ , so  $U''$  is negative due to which  $\Delta\nu$  becomes negative and hence there is a red shift.

The result can be generalized for polyatomic molecules. So, a high-frequency mode in a polyatomic molecule such as stretching modes, which is a small amplitude mode, imitates loose cage and suffers a redshift. While the low-frequency modes of high amplitude like bending mode resemble a tight cage and show a blue shift. Vibrational mode assignment and interpretation of spectra becomes easy by understanding the analytic-matrix interactions.

In addition to the matrix effects, there are several other phenomena such as aggregation, rotation of a guest molecule in the matrix cage and presence of multiple trapping sites that causes variation of matrix isolated spectra with respect to the gas phase spectra of the molecule. These are briefly discussed in the following section.

### 2.3.2 Multiple trapping sites

Interstitial and substitutional sites are the potential trapping sites for the guest species. All guest molecules do not get trapped in identical sites. The small size of interstitial sites allows the guest species to occupy them; monoatomic positive ions are most likely to occupy such sites. In substitutional sites, host species is replaced by the guest species. The matrix isolated species

occupies different substitutional sites depending on their size and shape. So, the guest molecule experiences different kinds of environment and gets perturbed differently inducing different shifts. As a result, instead of a single intense peak, a multiplet structure is observed with intensity proportional to the stability of each trapping site. The multiplet features observed due to the different matrix sites is called a site effect. Different matrices have different sites so the spectral features arising due to site effect can be identified by changing the matrix gas. For example effects due to inhomogeneous environment and the possibility of having multiple trapping sites is greatly reduced in a  $p$ -H<sub>2</sub> matrix.

### 2.3.3 Aggregation

An ideal matrix isolation experiment is one where the guest molecule is completely isolated in a matrix cage. Some of the Factors governing the isolation of guest molecule are the deposition rate, the deposition time and the guest to host ratio.

High guest to host ratio usually 1:1000 helps in achieving a high degree of isolation. At higher ratios, the molecule might aggregate to form dimer, trimer or multimer, so in addition to monomers, these aggregates might also get trapped in the matrix and induce different kinds of spectral effects such as broadening, slight shifts. These features can be identified by performing concentration-dependent (varying matrix ratio) and warm-up experiments (warming the matrix) in which monomer is made to diffuse and form dimers and high multimers. Different spectral features might also arise if two species are trapped very nearby resulting into the overlap of their respective cages which modifies the vibrational band.

We can calculate the probability to ensure maximum isolation of the host molecule. If the host species such as Carbon monoxide(CO) molecule occupies one substitutional site then the probability of finding another CO molecule near it is given as,

$$p = (1 - r)^{12}$$

where  $r$  is the reciprocal of matrix ratio. For a higher matrix ratio  $r$  is small so the above expression reduces to:

$$p = 1 - 12r$$

A matrix ratio of 1:1000 gives effective isolation of 99%. Contrary to the result of this analysis, it has been found experimentally that various dimers, trimers and higher aggregates of

CO are also formed at this matrix ratio. Another example is of Li atoms that dimerize even at a matrix ratio of 1:10,000 if the deposition rate is not fast.

#### **2.3.4 Lifting of the degeneracy of vibrational levels**

Matrix effects can also occur depending on the symmetry of the site. The trapped molecules get perturbed differently in different sites. Degenerate vibrational bands split in the matrix, if the molecule is trapped in the asymmetric site, lifting the degeneracy of the vibrational band. The effect has been observed for CO<sub>2</sub> and C<sub>2</sub>H<sub>2</sub> in N<sub>2</sub> matrix.

#### **2.3.5 Rotation of guest molecule in matrix cage**

The trapped molecules in an inert matrix at very low temperatures are expected to show no rotations. But, actually, the rotations are not completely absent. It is reported that some small molecules such as ammonia<sup>25</sup>, water<sup>26</sup>, alkali halides<sup>27</sup> and methanol<sup>28</sup> show rotation in some inert matrices. This is because noble gas matrices with large cavities provide a site for the molecules to rotate and cause multiplet splitting. For example, ammonia and water show rotations in Ar matrix but not in N<sub>2</sub> matrix. These rotational features can be identified by temperature cycling. Variation of temperature causes changes in population in rotational energy levels leading to a reversible intensity variation.

### **2.5 Advantages of Matrix Isolation and its Limitations**

Matrix isolation technique provides with an uncongested spectrum together with sharp linewidths. The isolated guest molecule in a rigid cage is free of any rotations, collisions, Doppler broadening, and spectral congestion, thus enables us to obtain spectra of sharp spectral line widths as compared to the spectra obtained using solid and liquid samples. The trapping of molecules at very low temperatures (~2-20 K) ensures that only the lowest electronic and vibrational levels are populated.

The absence of rotational lines and hot bands simplifies the spectra compared to that in the gaseous phase. As the sample is deposited onto the substrate during deposition, the amount of sample required is much smaller than typically used in experiments using flowing gases. The vibrational shifts ranging from ~2 cm<sup>-1</sup> for weak hydrogen bonded complexes to ~800 cm<sup>-1</sup> for very strong hydrogen bonded complexes is observed. These small line widths enable one to study small perturbations due to very weak intermolecular interactions, thereby offering a great advantage to study H-bonding and van der Waals interactions.

Another advantage of matrix isolation is that reactive intermediates that can't be studied by in-situ generation or require photolysis or some form of radiolysis for their formation can also be investigated by producing them before quenching with an excess of host gas on a cold surface.

The technique has various limitations such as it can be used to study only those species that are volatile at reasonable temperatures, without decomposition. This sets the limit on the size of the guest species that can be studied. Thus many interesting compounds such as biologically relevant molecules can't be studied in their native forms. Another problem is *cage effect*, in which the fragments produced by cleavage of precursor remain trapped in the same matrix cage that may undergo recombination.

## 2.6 Matrix Isolation Infrared Setup

The experimental setup combines the matrix isolation technique with the infrared spectroscopy to elucidate information about the vibrational features. The main components of matrix isolation setup involve:

- a). Cryostat
- b). Vacuum system
- c). Sample Chamber and deposition unit
- d). Fourier Transform Infrared(FTIR) spectrometer

### a). Cryostat

The heart of the technique is in the cryogenic systems that provide the cryogenic temperature for the deposition of the matrix.<sup>14</sup> A closed cycle cryostat using Hydrogen, Helium as a working fluid can achieve temperature up to 20 K, 10K respectively. In our experiments, the KBr window mounted within the cryostat reaches ~12 K using closed cycle He compressor cooled cryostat CH-202w/HC model (Sumitomo Heavy Industries Ltd.), which works on the principle of Grifford-McMohan (GM) refrigeration cycle. These devices consist of an expander, a compressor, vacuum shroud, and radiation shield.

The expander is the tip of the cryostat that attains a temperature of around 10 K. It is also known as the cold head of cold finger, where a GM refrigeration cycle takes place. Gifford McMahan Refrigeration Cycle: The rotation of the valve disk opens and allows the high pressure He gas to pass through the regenerating material into an expansion process. The difference in

pressure drives the piston to move upward allowing the gas at the bottom to expand and cool. As a consequence of which the low-pressure path is opened up by the rotation of valve disk. This path then allows the cold gas to flow through the regenerating material that results in heat extraction process and consequently also in cooling. Finally, the pressure difference causes displacer to move back to its original position, and the cycle is completed.

The expander is then linked to the compressor by two gas lines. One of the gas lines introduces high pressure. He gas to the expander while the other line returns the low-pressure gas from the expander. The cold end of the expander is surrounded by the detachable and rotatable vacuum shroud to avoid any collisional heat transfer to the expander due to conduction and convection. The vacuum shroud is made of stainless steel so that it does not adsorb water and thus limits the heat load on the expander. Since the cooling occurs in three stages, the first expansion stage of the cryostats achieves a temperature of  $\sim 25\text{-}30\text{ K}$ , usually fitted with a detachable radiation shield which is constructed using high purity copper and extends over the second stage to protect from room temperature thermal radiations emitted from the vacuum shroud.

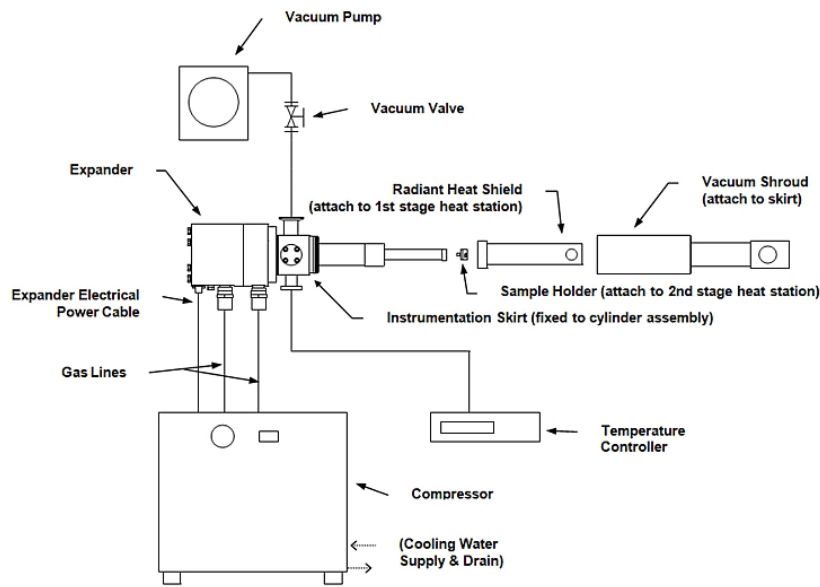


**Fig 2.3:** Schematic of closed cycle cryocooler

Several other support components are also needed such as temperature controller, chiller. A chiller unit (3k W, Werner Finley) is required to remove the heat from the low pressure working fluid before returning to the compressor. Similarly, a temperature controller (Lakeshore

Instruments-Model 335) is used to measure and adjust the temperature of the sample deposited on the window. Fig 2.3 shows a general schematic for a closed cycle cryocooler. The cryostat and its associated units are seen in Fig 2.4.



**Fig. 2.4:** Cryostat and its associated units

#### **b). Vacuum system**

A high vacuum ( $10^{-6}$  torr) is needed to evacuate the setup to obtain a spectrum devoid of impurities. The conditions for Matrix Isolation technique are achieved at very low temperatures and very high vacuum conditions. The desired vacuum can be achieved by using a variety of pumps as per the choice and the experimental conditions required.

In our experimental setup, a pressure of  $10^{-6}$  mbar is achieved using a mechanical rotary pump (Edwards, Diffstak MK2 series 100/300) followed up by a vapor diffusion pump (Hind Hivac: ED6). Rotary pump as shown in the Fig. 2.5(a) prepares a rough vacuum, by operating at a pumping speed of 200L/min and brings down the pressure from atmospheric pressure to  $10^{-3}$  mbar. It consists of a housing, vanes, an eccentrically installed rotor, an inlet, and an outlet, a working chamber and an outlet valve. As the rotor attached to the motor turns, the gas flows into the

enlarging suction chamber until it is sealed off by the second vane. This is followed by the compression of the enclosed gas until the outlet valve opens against the atmospheric pressure. The diffusion pump requires to be backed by the rotary pump and the two pumps together achieve a pressure of  $\sim 10^{-6}$  mbar.

Diffusion pump consists of a chamber with an oil vessel, a heater, a nozzle, and a chimney. A simple schematic is shown in Fig. 2.5(b). Its working is based on the momentous transfer to gas molecules from a directed jet of oil. The chamber's outside surface is wound by cooling coils that carry water. The heater vaporizes the oil that rises into the vapor chimney, which is then deflected downwards by the nozzles imparting momentum to randomly moving gas molecules in the chamber. Momentum deflects the molecules in a random direction towards the pump exit, thereby creates a vacuum. The walls of the pumps are cooled by water from the chiller (Winker-Finley) so that the molecules of the working fluid vapor condense before their motion is randomized by repeated collisions.

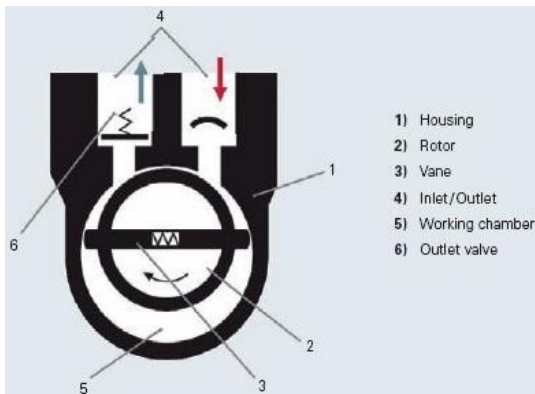


**Fig. 2.5(a):** Rotary vane pump

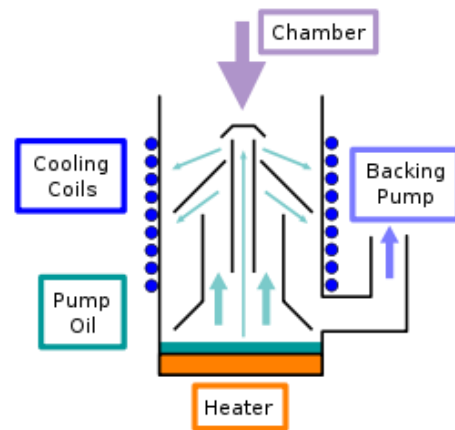


**Fig. 2.5(b):** Schematic of oil diffusion pump

The vacuum created inside the system is measured using a Pirani Gauge 26 (Edwards APG 100Active Pirani Gauge) and a digital Penning Gauge (Hind Hivac) as shown in Fig. 2.6. Pirani works on the principle of thermal conductivity while Penning gauge is an ionization gauge.



**Fig. 2.6(a):** Pirani gauge

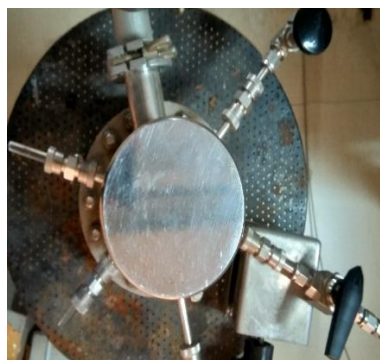


**Fig. 2.6(b):** Penning gauge

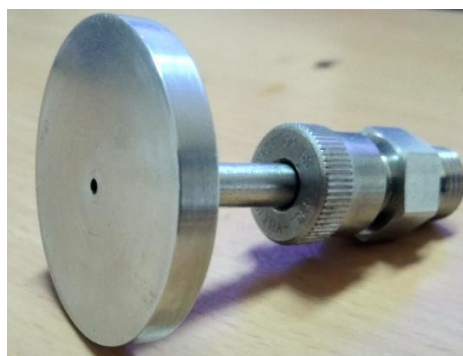
### c). Sample chamber and deposition technique

The nature of the sample decides the method of depositing the sample on the substrate. Matrix isolation technique can only be employed for the study of those species which are volatilizable without decomposition, thus set a limit on the size and the thermal stability of the species to be studied. The sample molecules can be deposited when pressure of the system comes down to  $\sim 10^{-6}$  mbar and the temperature of the KBr window reaches 12 K. The matrix host gas and the sample of interest are usually pre-mixed in a guest to host ratio of 1:1000 in the mixing chamber and is deposited through a single effusive nozzle. The mixing chamber is a 1L stainless steel cylindrical chamber with several ports for sample introduction and pumping. The volatile species can be deposited either by a double jet nozzle (for liquid samples) which one nozzle effuses matrix gas while the second nozzle introduces the sample into the vacuum system or by a single jet nozzle (for liquid or solid sample).

First, the matrix gas ( $N_2$  or Ar) is filled into the chamber to the desired pressure. The mixing chamber is then connected to the cryostat connecting using Cu tubing and a sample holder containing 2-Butyne 1, 4-diol. Cu tubing was connected to the mixing chamber at one end while at another end to the sample holder which was then connected to the cryostat so that the matrix gas carries along with it the vapors of the solid sample and deposit the sample/matrix on the cold KBr substrate. The flow rate during deposition was controlled using a needle valve (Model: EVN 116, Pfeiffer Vacuum) which was typically maintained at  $\sim 3$  mmol/hr connected to an effusive nozzle. The vacuum shroud was mounted in the sample container of FTIR spectrometer. The expander was rotated within the vacuum shroud from deposition mode to observation mode when an observation was to be made. Fig. 2.7 shows the sample introduction assembly.



Mixing Chamber



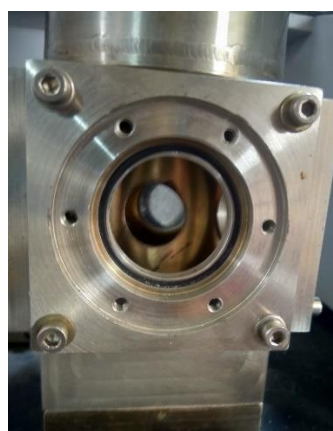
Effusive Nozzle



Pressure Gauge



Needle Valve



KBr Window

**Fig.2.7:** Sample introduction assembly

#### **d). FTIR spectrophotometer**

An FTIR spectrophotometer works by the excitation of the vibrational modes of a molecule by shining infrared light on the sample. The sample is loaded onto substrates such as KBr, CsI which are usually transparent in the  $400\text{-}4000\text{cm}^{-1}$  region. An IR spectrum of a sample can be obtained using different methods like a thin film, KBr pellet, Attenuated Total Reflection (ATR), and diffuse reflectance (DRIFT). In this, an incident beam falls over the sample which absorbs specific wavelength in the beam that corresponds to the frequencies of the IR active normal modes of the sample molecule. The resultant transmitted beam is then directed on the detection unit which is then Fourier-Transformed to yield the IR spectrum of the sample. The general layout of an FTIR spectrophotometer is shown below which works on the principle of a Michelson interferometer.

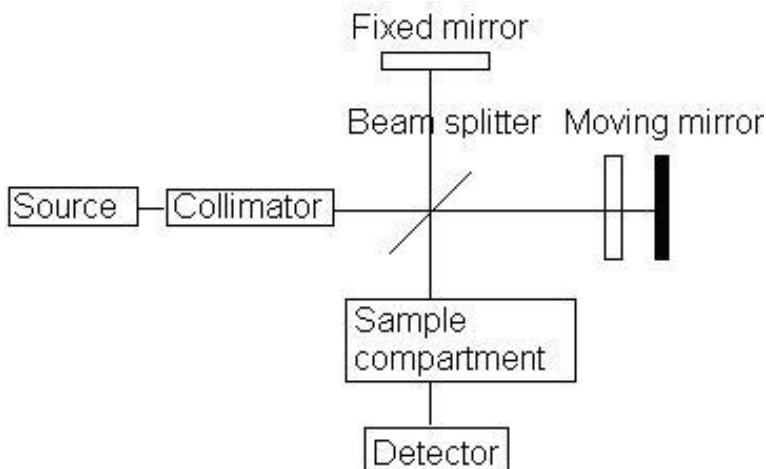


**Fig. 2.8:** Schematic diagram of FTIR spectrophotometer

A Bruker-Tensor 27 FTIR spectrophotometer was used to study the matrix isolated molecules. High resolution of  $0.5\text{ cm}^{-1}$ , multiple scans (8 scans) in a spectral region of  $4000$  to  $400\text{ cm}^{-1}$  were used to obtain a good signal to noise ratio. Firstly, a reference spectra at  $12\text{ K}$  is recorded then a spectrum of matrix isolated molecule is recorded. Then the temperature of the matrix was raised to  $27\text{ K}$  when using  $\text{N}_2$  for the experiment. This process of raising the temperature and allowing diffusion, remove unstable sites, allows the complex formation followed by cooling is called annealing. The matrix is then cooled back to  $12$  to obtain annealed spectra.

A home-built matrix isolation setup is shown in Fig. 2.9.

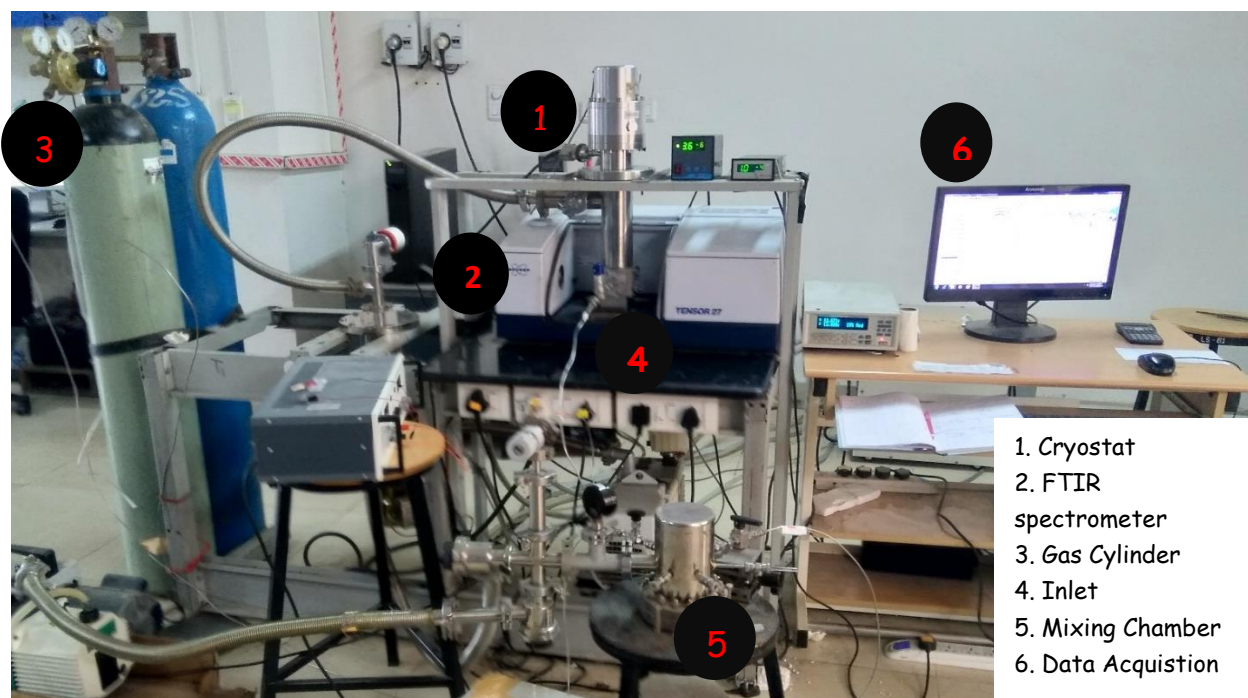


**Fig. 2.9:** Home-built matrix isolation set-up at IISER

## 2.7 Computational Methods and Procedures

The experimental studies on the species of interest are supported by computational work. Computations were performed using Gaussian09<sup>29</sup> package to obtain molecular properties such as structures, energies, and frequency calculations.

### 2.7.1 Level of theory

Several theoretical methods are available, each with a different approximation for *ab initio* calculations. The choice of method to be used depends on the system under study. Table 1 provides examples of different methods that can be used in Gaussian09. A brief discussion of these is presented in sections below.

**Table 2.1:** Level of theories

METHOD	EXAMPLES
SEMI-EMPIRICAL METHODS	PM6, AM1
HATREE- FOCK	HF
MOLLER-PLESSET PERTURBATION THEORY	MP2, MP3
DENSITY FUNCTIONAL THEORY	BLYP, B3LYP, M06X, M06-2X
COUPLE CLUSTER METHODS	CCSD(T)

The computations are first done at the Hartree-Fock (HF) level to which electronic correlations effects are added to improve the accuracy. These are non-variational methods and treat the correlation potential using Rayleigh-Schrodinger perturbation theory to second (MP2), third (MP3) and fourth (MP4) order. Studies on MP theory show that at higher orders it is not necessarily convergent. Though MP2 energy corrections usually overestimate bond energies. Molecular properties calculated at MP3, MP4 level are not much improved than MP2 even for small molecules. This is because the first order correction  $W_1$  is smaller for the excited state than for the ground state, making  $\lambda$  negative that raises the ground state energy over the excited state energy. The energy separates at  $\lambda = 0$  can be overcome and result in divergence

$$E(\lambda) = \sum_{i=0}^{\infty} W_i \lambda^i$$

The electron correlations are included in DFT (Density Functional Theory) methods by using electron density functionals rather than wavefunction producing more accurate results than HF.

Two major types of DFT methods is the pure and hybrid DFT methods. Pure method involves two functionals corresponding to correlation and exchange while the hybrid functionals have some HF exchange included in it like BLYP(Beck-Lee-Yang-Pee).

The most commonly used hybrid DFT is B3LYP that includes Becke three parameter non-local exchange functionals with a non-local correlation of Lee, Yang, and Parr<sup>30</sup>.

Minnesota functional (M06) are modified DFT functionals constructed by mixing HF and DFT exchange terms with an empirical fitting, but constraining to a uniform electron gas. The different amount of HF exchange gives us different functionals such as M06-L, M06-2X. The choice of functionals varies as per the system under study such as M06-L with 0% exchange is accurate for transition metal thermochemistry while M06-2X with 54% of HF exchange is employed best for Main group thermochemistry and non-covalent interactions. M06-2x method has been widely employed for the ab-initio study of this system.

The coupled cluster method starts with HF-Molecular orbital method and corrects by adding electron correlation methods similar to MP methods. They provide qualitatively correct data but with very high computational cost, then too CCSD(T) has become the “ gold standard of quantum chemistry.”

### 2.7.2 Basis sets

Basis sets is a collection of mathematical functions to build quantum mechanical wavefunction for a molecular system. In a physical sense, the basis set specifies the region of space to which an electron is restricted. Larger the basis set more accurate are the results, as there are lesser constraints for the electrons in region of space but with a finite probability of finding an electron in the region of space. Broadly, there are eight types of basis sets. The choice of basis set depends over the system under investigation, computation time and the resources needed.

A minimum basis set is one in which a single basis set function is used for each orbital in an HF calculation on the free atom. The most common minimum basis set is STO-nG where ‘n’ is an integer. This n represents the number of Gaussian-type orbitals (GTOs) required to approximate

STO for the core and valence orbitals. But, the inflexibility for an accurate representation of orbitals provides less accuracy.

**Table 2.2:** Basis sets

<b>TYPE</b>	<b>EXAMPLES</b>
MINIMAL BASIS SETS	STO-3G, STO-6G
SPLIT VALENCE BASIS SETS	4-21G, 6-31G, 6-311**
CORRELATION CONSISTENT BASIS SETS	cc-pVDZ, cc-pVTZ, cc-pCVDZ
POLARIZATION CONSISTENT BASIS SETS	def2-SV(P)
COMPLETE BASIS SETS(CBS)	
PLANE WAVE BASIS SET	co-type
REAL SPACE BASIS SET	

The extended basis sets use three to four Slater orbitals hence are more accurate. The split valence type basis sets also called as Pople's basis set n-ijkG use Gaussian functions of different sizes to estimate the inner orbitals and STOs. However, the basis functions with different shapes are not allowed. Polarization basis sets overcome this limitation by adding orbitals with angular momentum exceeding what is required. These functions are important for reproducing chemical bonding and should be included where the electron correlations are important. In Pople's sets, they are represented with asterisk, i.e. 6-311++G (d, p) will be represented as 6-311G\*\*. There are two polarization functions on non-hydrogen atoms (2d) and one additional polarization on hydrogens (p) while '++' imply diffuse function on Hydrogen and non-hydrogen atom and.

The most widely used basis sets are the complete basis sets (CBS) that have become the current state of the art for correlated calculations. These are designed to converge systematically to complete basis set limit using extrapolation techniques. The basis sets are cc-pVNZ where N=D, T, Q, 5, 6... (D=double -zeta, T=triple-zeta) and 'cc-p' stands for correlation consistent polarized while 'V' indicates valence only basis sets. The 'aug' adds one diffuse function on each atom. Two of the most commonly used basis sets in this work are 6-311G\*\* and aug-cc-pVDZ.

### 2.7.3 Geometry optimization and frequency calculation

The first step in the computational study of a molecule is the geometry optimization to locate minimum energy structure on potential energy surface referred to as stationary point (SP). This is done using ‘OPT’ command in Gaussian09 package. Geometry optimization locates the stationary point which is closest to initial guess geometry. Hence, initial guess geometries by varying dihedral angles and bond angles were given as an input to obtain various possible conformers. The successful optimization is the one which locates the SP, where the forces are zero. The convergence criteria defined by Gaussian 09 to locate SP is when the forces, the calculated displacements, and the root mean square of displacement falls below a certain threshold value. All the computations were performed using MP2, and DFT (M06-2X, B3LYP) methods and aug-cc-pVDZ basis sets on Fujitsu workstation.

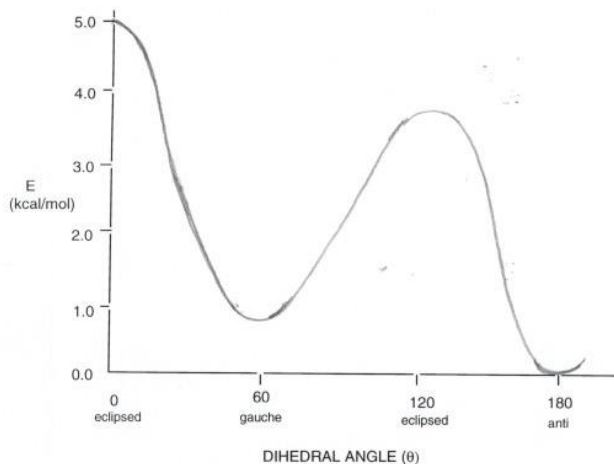


**Fig. 2.10:** Optimization based on energy

A successful optimization can locate SP, but it might not be the intended minima. A geometry optimization contains no information about the nature of SP so; it is possible that the located SP might be a global minimum or a saddle point. Thus, to distinguish between global minima and local minima, harmonic frequency calculations are performed on optimized geometries at the same levels of theory. For minima, all the computed frequencies should be positive. Structures with imaginary frequencies are considered as saddle points. Frequency calculations can be done by combining the opt command with the frequency command (‘OPT+FREQ’) which provides the (computed) vibrational spectra for the optimized geometry along with the energy value

The computed frequencies are first scaled using scaling factors determined by bringing the computed values in agreement with the experimental values. Then a computed spectrum is plotted by using scaled frequencies and the intensity values obtained from the output files. The plotting was done using SYNSPEC<sup>31</sup>, as Lorentzian curve with a full width at half minimum (FWHM) of 1.0 cm<sup>-1</sup> and a step size of 0.1. These plots have been presented in comparison with the experimental spectra in the next chapter.

#### 2.7.4 Energy calculations

Energy is an essential criterion when studying complexes. A super-molecular approach was employed to calculate the interaction energies denoted by  $E$ . The interaction energy between two atoms or molecules A and B is calculated as the energy difference between the product complex AB and its monomers A and B which is given as:

$$E_{int} = E_{AB} - (E_A + E_B)$$

Where  $E_A$ ,  $E_B$  and  $E_{AB}$  are the energies of the monomer A and B and the complex formed between A and B respectively.

Negative interaction energy indicates that the complex formed is stable relative to its monomers. The lowest energy any quantum system can have is the zero point energy. In semi-empirical methods, the zero point energy is already included in the output energy value but for the ab-initio methods used in this work, the zero point corrections provided separately in the output file. These corrections were then added to the absolute energy values to obtain zero-point corrected interaction energy values, represented as ZPE.

$$E_{ZPE} = E + ZPE$$

For systems involving dispersion interactions or hydrogen bonds, the interaction energy value is often very large. This is because the wavefunction of the monomer is expanded in lesser basis set functions than the wavefunctions of the complex. As a result, complex is stabilized more than the monomers. Hence, the inconsistent treatment of the monomers gives rise to an error, known as basis set superposition error and can be eliminated if the monomer A is allowed to use additional basis function from the monomer B and vice-versa. Typically the counterpoise (CP) method, proposed by Boys and Bernadi is employed for removing BSSE.<sup>32</sup> To calculate the energy of monomer A,  $E_A^{AB}$  by employing CP method, the basis functions on monomer B on all its atomic centers are used, while neglecting their electronic and nucleic charges. These basis

functions are called ghost function and, the atoms of B are called the ghost atoms. In the same way, energy of monomer B,  $E_B^{AB}$  is also calculated. The BSSE corrected interaction energies are represented as:

$$E_{BSSE} = E_{AB}^{AB} - E_B^{AB} - E_B^{AB}$$

Where the subscript represents the chemical system considered, monomer or the complex while, the superscript represents the basis used.

MP2 complete basis set limit interaction energies were also calculated using a two-point extrapolation method by Helgaker *et al.*<sup>33</sup>

$$\Delta E_{MP2/CBS} = \frac{4^3 \times \Delta E(pVQZ) - 3^3 \times \Delta E(pVTZ)}{4^3 - 3^3}$$

An intense care should be taken while analyzing the output energy values; it is that a comparison of absolute energies must be done only across the same levels of theories. Also, energy comparison is not possible when the total number and the types of atoms are different for the two systems under consideration.

#### 2.7.4 Atom in molecules analysis

The presence of Hydrogen bonding can be determined using Bader's theory of 'atoms in molecules' which uses electron based topology<sup>34</sup>. This used the electron density mapping to define a bond. In this thesis, AIM analysis was performed to unravel weak non-covalent interactions such as O-H... $\pi$ , hydrogen bonds, etc.

<sup>22</sup>Since any interaction between the two nuclei affects the charge density  $\rho(r)$ . The points in the space where the first derivatives of  $\rho(r)$  vanishes, i.e.  $\nabla \rho, (r) = 0$  referred as the bond critical points (CPs). The sign of second the derivative determines whether the point is a minima, a maxima or a saddle point.

The software obtains the charge density and the corresponding Laplacian  $\nabla^2(\rho)$ , by choosing a coordinates axis arbitrarily to generate a  $3 \times 3$  Hessian matrix. The matrix is then diagonalized to obtain three eigenvalue  $\lambda_1, \lambda_2, \lambda_3$  that are summed up to get a Laplacian which plays an important role in the characterization of chemical bonding. A CP is defined in terms of rank ( $\omega$ ) and signature( $\sigma$ ), where  $\omega$  denotes the number of non-zero eigenvalues and  $\sigma$  is the algebraic sum of the signs of eigenvalues. A (3, -1)CP exists when there is chemical bond

between two nuclei hence is a bond critical point (BCP) while a (3, +1) CP is found in the interior of the ring and is known as ring critical point (RCP), a (3, +3)CP is a cage critical point (CCP) and a(3, -3)CP correspond to a minima. The number of CPs that can co-exist in a system with a finite number of nuclei, are governed by Poincare-Hopf relationship given by:

$$n - b + r - c = 1$$

Where n is the number of nuclei, b, r and c is the number of BCPs, RCPs, and CCPs respectively.

A pictorial representation of this process is attached below. As seen in the figure, when moving in the x-direction, a sudden rise is seen in the electron density when it reaches atom 1 (dark red) which starts to decrease as it starts approaching the mid-point of the F-F distance. The density increases again when it reaches atom 2. The variation in color depicts the variation in electron density. Hence, exactly at the mid-way (in this case) between the two atoms, there exists a minimum, in terms of electron density. Now, on moving along either y- or x-axis, the electron density is zero until it reaches near the atoms where it increases. Electron density again decreases and becomes zero ones it has crossed the atom. Hence in between the two atoms there exists a minimum (double derivative is zero from one direction while maxima from the other two directions).

Gaussian 09 was used to generate wavefunction file from the optimized geometries which can be used as input for AIM2000<sup>35</sup> software. To confirm hydrogen bonding, the charge density values were examined to be within the range 0.002-0.034 a.u. and  $\nabla^2(\rho)$  in the range 0.024-0.139 a.u. at the BCP as suggested by Koch and Poplier<sup>36</sup>.

#### 2.7.4 Localized molecular orbital energy decomposition analysis

Intermolecular interactions are an important factor in the formation of different systems.<sup>37</sup>EDA is a novel approach to quantify chemical effects that partition the intermolecular interaction energy into various energy components such as electrostatic, polarization, charge transfer, etc. This interaction energy can be decomposed by employing different approaches depending on the type of the interactions under consideration. EDA can be implemented to analyze covalent as well as intermolecular interactions. Total interaction energy can be decomposed as follows:

$$\Delta E_{int} = E_{elec} + E_{exc} + E_{rep} + E_{pol} + E_{dis}$$

These terms can be defined as below:

1. Coulombic interaction( $E_{elec}$ ) : It gives a localized interaction energy between the occupied molecular orbitals.
2. Exchange ( $E_{exc}$ ): the interaction between occupied molecular orbitals that causes electron exchange and delocalization between the molecules.
3. Repulsion( $E_{rep}$ ) : the interaction arising due to Pauli's exclusion principle and is repulsive in nature.
4. Polarization( $E_{pol}$ ): this interaction involves mixing between the occupied and the vacant molecular orbitals of the molecules.
5. Dispersion( $E_{dis}$ ): this interaction energy is due to instantaneous and induced dipole interactions.

In this work, EDA was employed to understand the nature of interactions in the hydrogen-bonded complexes at the MP2 level of theory. The systems with the n- $\sigma^*$  type of interactions have the electrostatic terms in dominance, whereas dispersion and polarization terms dominate in the systems consisting of H-bonding interactions.

### 2.7.5 Natural bond orbital analysis

<sup>38</sup>NBO is a helpful tool in understanding the delocalization of the electron density, hyperconjugation effects and majorly both the intermolecular or intramolecular interaction. It is used to understand and quantify the hydrogen bonding interactions occurring when there is an orbital overlap between donor and acceptor. A stable donor-acceptor interaction occurs when there is delocalization of electron density between the occupied (bond or lone pair) NBO orbitals and unoccupied (antibonding or Rydberg) orbitals. The basis of NBO analysis is to transform a given wavefunction into a localized form, i.e., to the lone pair (one-center) and bond (two-center) that draws a Lewis-like picture. The program analyzes a many-electron molecular wavefunction in terms of localized electron-pair bonding units. It achieves this by transforming the input atomic orbitals into natural bond orbitals (NBOs) via natural atomic orbital (NAOs) and natural hybrid orbitals(NHOs).

NBO analysis was performed to understand the role of orbitals in the stabilization of particular conformers and elucidate hydrogen bonding interactions in water- complexes. The output files from the MP2 level of theory were used to perform NBO analysis by using pop=fullnbo keyword through the Gaussian09 package. The NBO output files gives us second-order perturbation energies E to determine the extent of interaction between the donor and acceptors which depends on the orbital overlap F(i,j) between the donor and the acceptor orbitals and is

inversely proportional to energy difference between the donor-acceptor  $[E(i)-E(j)]$ . Hence, a higher value of  $E$ , more will be the donating tendency of a donor. Vibrational shifts in the spectrum can also be understood using the NBO analysis. For example, when there is a transfer of electron density from a bonding orbital to an antibonding orbital a redshift is observed in the IR spectrum.



## Chapter 3

### Results and Discussion

2-Butyne-1,4-diol is a multifunctional molecular system that extensively used as an external intermediate in the synthesis of polyols, pharmaceuticals. The multiple hydrogen bonding sites due to different functional groups provide a rich conformational landscape and to study competitive hydrogen bonding. The section presents a conformational analysis of the 2-Butyne-1,4-diol system through experiments corroborated with the ab-initio computations.. Later we will discuss our studies on the complexes of BYD with H<sub>2</sub>O. All the computations were performed using Gaussian09 suite of the program, followed by NBO and, AIM analysis.

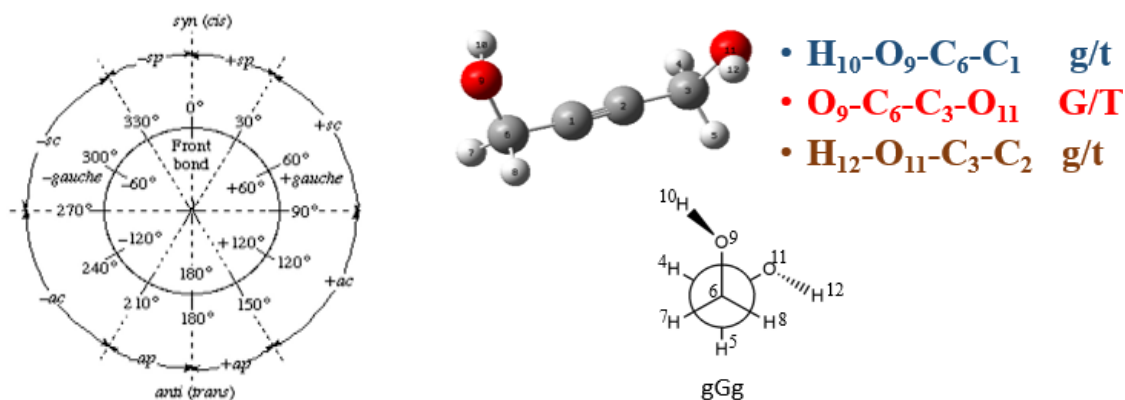
#### 3.1 2-Butyne-1,4-diol

##### 3.1.1 Computational results



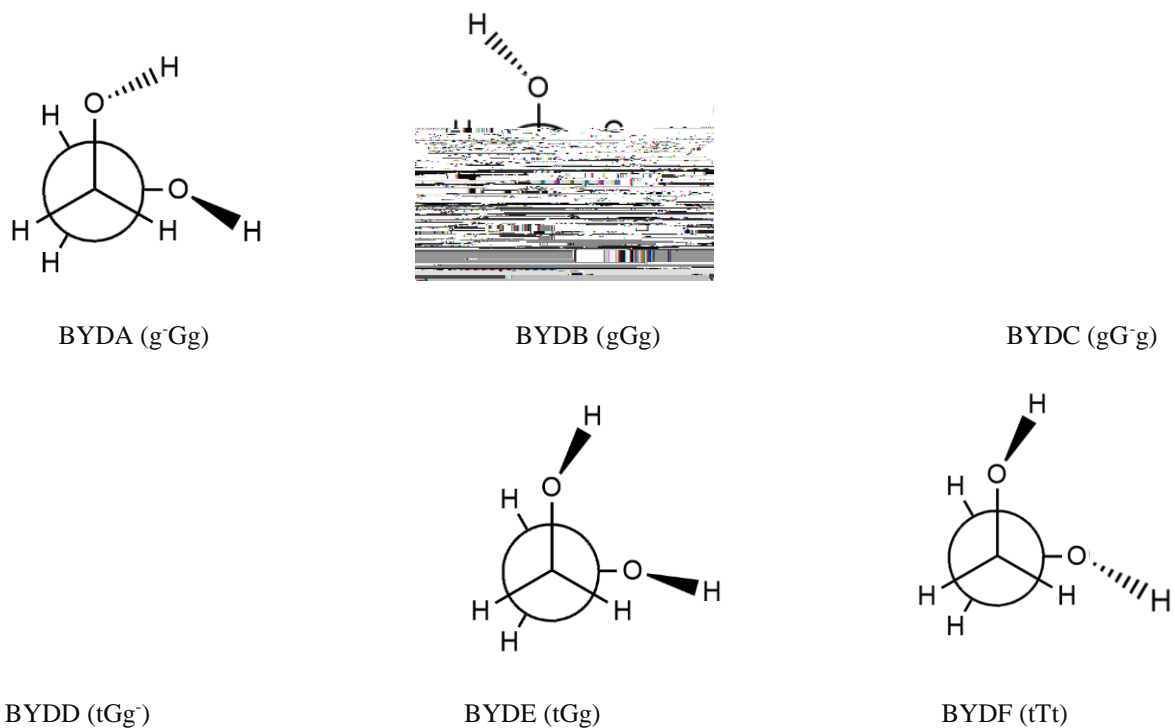
**Fig. 3.1:** 2-Butyne-1,4-diol

Fig 3.1 shows that 2-Butyne-1,4-diol has the possibility of multiple conformations due to the presence of two –OH groups and an acetylene moiety between the two OH groups. The two hydroxyl groups and C-O groups attached to the alkyne moiety through a C-C single bond have rotational degrees of freedom which give rise to multiple geometrical conformations of this molecule. These conformations were then classified into two major classes based on the two C-O bonds being oriented either gauche(G) or trans(T) to each other and on orientation of OH group along the C-C bond. The nomenclature used to label these geometries is the same as followed by the Radom et al<sup>39</sup> and is shown in Fig. 3.2. The notation g<sup>-</sup> and g indicates the orientation of the OH group in the acetylenic plane. In example provided in Fig 3.2, the two OH groups are gauche to C-C bond, while OCCO dihedral angle is also gauche thus the conformer is gGg. Similarly by varying these parameters different conformers were obtained which then were optimized at the MP2 and M06-2X levels of theory, employing 6-311++G\*\* and aug-cc-pVDZ basis sets.



**Fig. 3.2:** Nomenclature for the notation of 2-Butyne-1,4-diol conformations

Six geometries were optimized at MP2/aug-cc-pVDZ, as displayed in Fig 3.3. Out of these six geometries, three lowest energy conformers are gauche while the others were found to be trans. The structures along with their notation are presented in the Fig.3.2. The dihedral angles for the conformations are provided in the appendix.



**Fig. 3.3:** Conformations of 2-Butyne-1,4-diol

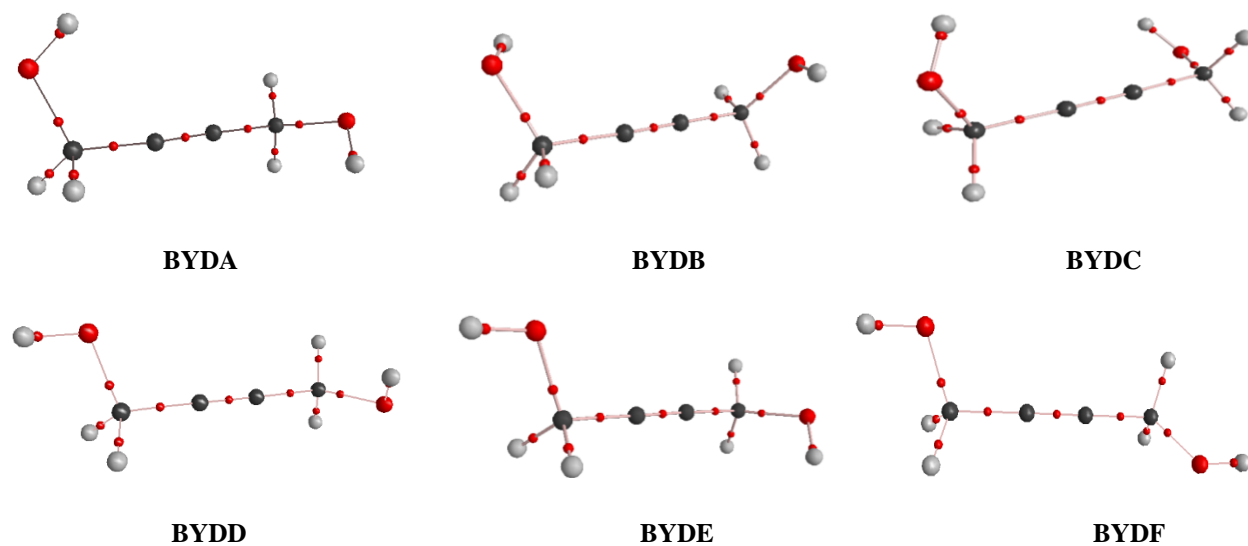
The relative energy ordering for the various conformers at MP2 and M06-2X levels with 6-311++G\*\* and aug-cc-pVDZ basis sets is provided in Table 3.1. All the calculations at M06-2X method were done using the int=ultrafine options. The conformers at both MP2 and M06-2X

levels showed a similar energy ordering. The conformer labeled BYDA is found to be the most stable conformer. BYDB and BYDC are found to be nearly isoenergetic compared with BYDA.

**Table 3.1:** Relative energy ordering (kcal/mol)

Conformations	M06-2X		MP2	
	aug-cc-pVDZ	6-311++G**	aug-cc-pVDZ	6-311++G**
	Raw/ZPCE	Raw/ZPCE	Raw/ZPCE	Raw/ZPCE
BYDA	0.00/0.00	0.00/0.03	0.00/0.00	0.00/0.00
BYDB	0.11/0.01	0.12/0.06	0.09/0.06	0.10/0.06
BYDC	0.14/0.19	0.14/0.00	0.15/0.02	0.15/0.09
BYDD	1.51/1.41	1.74/1.51	1.25/1.12	1.66/1.37
BYDE	1.85/1.67	2.18/1.82	1.62/1.42	2.06/1.74
BYDF	3.42/3.18	3.99/3.32	2.91/2.52	3.84/2.74

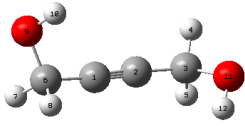
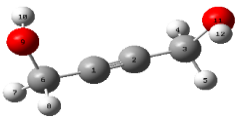
AIM analysis for the various conformers was performed, and the results are summarized in Fig. 3.4. AIM analysis revealed that there was no bond critical point BCP between two hydroxyl groups of diol, thereby indicating that there was no intramolecular (O-H...O) hydrogen bonding in the conformers of BYD. Thus, the AIM analysis ruled out the role of intramolecular O-H...O hydrogen bonding in the conformational landscape of BYD.

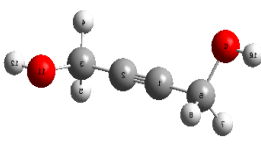


**Fig. 3.4:** AIM analysis of 2-Butynediol

Further, NBO analysis was performed to understand the role of orbital interactions in the conformational preferences in BYD. The NBO analysis for the three lowest energy conformers BYDA, BYDB, BYDC along with the highest energy conformer BYDF is provided in Table 3.2. Table 3.2 indicates second-order perturbation energies [E(2)] with energy values above the threshold of 0.5 kcal/mol.

**Table 3.2:** NBO analysis for BYDA, BYDB, BYDC and BYDF conformations

Conformation	Donor NBO(i)	Acceptor NBO(j)	E(2)	E(j)-E(i)	F(i, j)
			[kcal/mol]	[a.u.]	[a.u.]
 BYDA	LP1 O(9)	$\sigma^*C(1)-C(6)$	1.59	1.57	0.045
	LP2 O(9)	$\sigma^*C(1)-C(6)$	7.36	1.22	0.085
	LP1 O(9)	$\sigma^*C(6)-H(7)$	2.55	1.52	0.056
	LP1 O(9)	$\sigma^*C(6)-H(7)$	1.53	1.51	0.043
	LP2 O(9)	$\sigma^*C(6)-H(8)$	7.82	1.16	0.085
	LP1 O(9)	$\pi^*C(1)-C(2)$	0.70	0.83	0.021
	LP2 O(9)	$\pi^*C(1)-C(2)$	0.67	0.82	0.021
	LP1 O(11)	$\sigma^*C(2)-C(3)$	1.43	1.57	0.042
	LP2 O(11)	$\sigma^*C(2)-C(3)$	7.77	1.22	0.087
	LP1 O(11)	$\sigma^*C(3)-H(4)$	2.51	1.53	0.055
	LP1 O(11)	$\sigma^*C(3)-H(5)$	1.67	1.52	0.045
	LP2 O(11)	$\sigma^*C(3)-H(5)$	7.44	1.16	0.083
	LP2 O(11)	$\pi^*C(1)-C(2)$	0.53	0.83	0.019
	LP2 O(11)	$\pi^*C(1)-C(2)$	0.88	0.83	0.024
 BYDB	LP1 O(9)	$\sigma^*C(1)-C(6)$	1.59	1.57	0.045
	LP2 O(9)	$\sigma^*C(1)-C(6)$	7.33	1.22	0.084
	LP1 O(9)	$\sigma^*C(6)-H(7)$	1.52	1.51	0.043
	LP1 O(9)	$\sigma^*C(6)-H(7)$	7.85	1.16	0.085
	LP2 O(9)	$\sigma^*C(6)-H(8)$	2.53	1.52	0.056
	LP2 O(9)	$\pi^*C(1)-C(2)$	1.04	0.83	0.026
	LP1 O(11)	$\sigma^*C(2)-C(3)$	1.59	1.57	0.045
	LP2 O(11)	$\sigma^*C(2)-C(3)$	7.33	1.22	0.084
	LP1 O(11)	$\sigma^*C(3)-H(4)$	2.53	1.52	0.056
	LP1 O(11)	$\sigma^*C(3)-H(5)$	1.52	1.51	0.043
	LP2 O(11)	$\sigma^*C(3)-H(5)$	7.85	1.16	0.085
	LP2 O(11)	$\sigma^*C(1)-C(2)$	1.04	0.83	0.026

 BYDC	LP1	O(9)	$\sigma^*C(1)-C(6)$	1.49	1.57	0.043
	LP2	O(9)	$\sigma^*C(1)-C(6)$	7.63	1.22	0.086
	LP1	O(9)	$\sigma^*C(6)-H(7)$	1.62	1.52	0.044
	LP1	O(9)	$\sigma^*C(6)-H(7)$	7.58	1.16	0.084
	LP2	O(9)	$\sigma^*C(6)-H(8)$	2.52	1.53	0.055
	LP2	O(9)	$\sigma^*C(1)-C(2)$	0.69	0.83	0.021
	LP2	O(9)	$\sigma^*C(1)-C(2)$	0.69	0.83	0.021
	LP1	O(11)	$\sigma^*C(2)-C(3)$	1.43	1.57	0.043
	LP2	O(11)	$\sigma^*C(2)-C(3)$	7.63	1.22	0.086
	LP1	O(11)	$\sigma^*C(3)-H(4)$	2.52	1.53	0.055
	LP1	O(11)	$\sigma^*C(3)-H(5)$	1.62	1.52	0.044
	LP2	O(11)	$\sigma^*C(3)-H(5)$	7.58	1.16	0.084
	LP2	O(11)	$\sigma^*C(1)-C(2)$	0.69	0.83	0.021
	LP2	O(11)	$\sigma^*C(1)-C(2)$	0.69	0.83	0.021
 BYDF	LP1	O(9)	$\sigma^*C(1)-C(6)$	1.33	1.60	0.041
	LP1	O(9)	$\sigma^*C(6)-H(7)$	1.04	1.53	0.036
	LP1	O(9)	$\sigma^*C(6)-H(7)$	7.66	1.15	0.084
	LP2	O(9)	$\sigma^*C(6)-H(8)$	1.13	1.53	0.037
	LP1	O(11)	$\sigma^*C(2)-C(3)$	1.33	1.60	0.041
	LP1	O(11)	$\sigma^*C(3)-H(4)$	1.14	1.53	0.037
	LP1	O(11)	$\sigma^*C(3)-H(5)$	1.04	1.53	0.036
	LP2	O(11)	$\sigma^*C(3)-H(5)$	7.66	1.15	0.084

It can be seen that for BYDA conformer, there is significant contribution due to the delocalization of lone pair on O(9) and O(11) to the antibonding orbital of C(1)-C(6) and C(2)-C(3), respectively, with E(2) values of ~8 kcal/mol. Also, there is no contribution of lone pairs of O atom to the anti-bonding orbital of the O-H bond, consistent with the AIM results (Fig.3.4), clearly pointing to the absence of intramolecular hydrogen bonding. For BYDB and BYDC conformers, both the contribution from O(9) atom to C(6)-H(7) is ~8 kcal/mol as compared to smaller contributions of ~4 kcal/mol in BYDA. For BYDF, the contribution of lone pairs O(9) and O(11) to the anti-bonding orbital of C(1)-C(6) or C(2)-C(3) bonds is meager compared to the contributions observed for this delocalization in case of BYDA, BYDB, and BYDC. A weak O-H... $\pi$  interaction is also seen in case of BYDA, BYDB and BYDC of order ~1.2 kcal/mol. Thus,

NBO analysis further strengthens the claim that intramolecular hydrogen bonding is absent in the three lowest energy conformers.

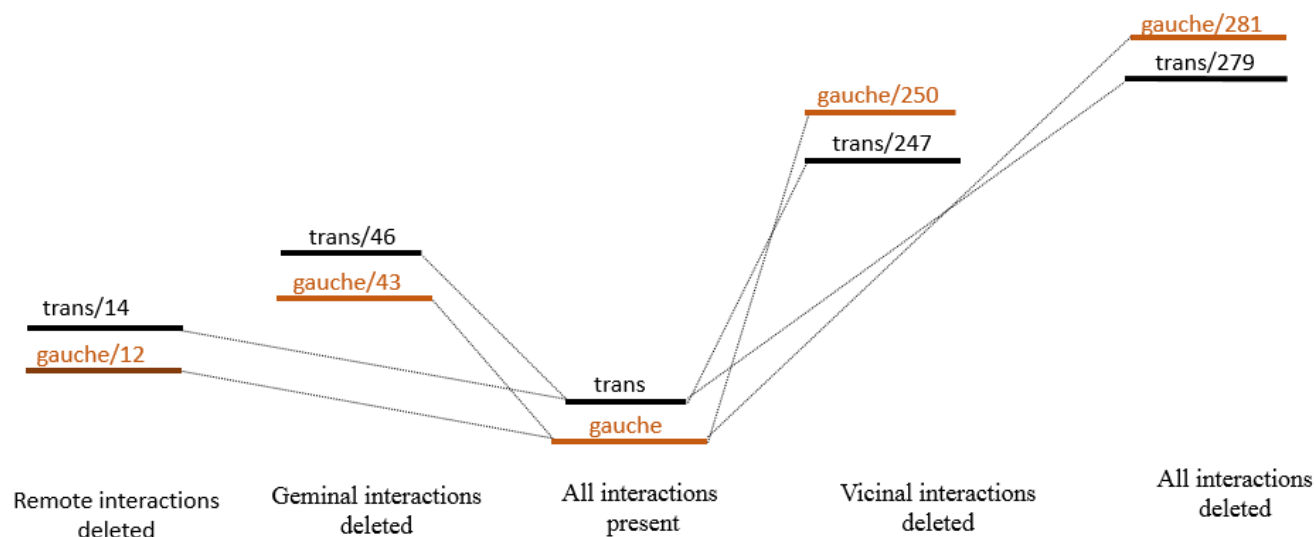


**Fig. 3.5:** Correlation diagram showing the energy (in kcal/mol) of gauche and trans conformer of BYD, at M06-2X/aug-cc-pVDZ when orbital interactions were systematically deleted.

The relative contributions of orbital interactions such as remote, germinal and vicinal delocalization interactions, in deciding the conformational preferences in BYD were quantitatively estimated by systematically deleting these interactions, and computing the energy of gauche and trans conformers. Natural Bond Orbital Deletion analysis provides an excellent approach to measure the bonding energy within a single molecular fragment or many. It sets specific elements of the Fock matrix to 0.00 and then re-diagonalizes it to find the difference in energy with respect to the original matrix. The syntax for its usage is `pop=nbodel` along with the keyword such as `NOVIC` or `NOGEM` which specifies the deletions to be performed. The relative changes in the energies due to systematic deletions of interactions are shown graphically in Fig 3.5.

The figure clearly shows that when all the interactions were present, the gauche conformer which includes BYDA, BYDB, and BYDC is lower in energy than the remaining trans conformers. When vicinal interactions were deleted (retaining the geminal and remote interactions), the highest energy conformer BYDF (tTt) turns out to be lower in energy than the gauche, meaning that there is a flip in the conformational preference of BYD. Deletion of vicinal interactions increases the energy of gauche conformer of BYD by ~250 kcal/mol and that of trans conformer by ~ 247

kcal/mol, which suggests that the vicinal interactions play a significant role in deciding the conformational ordering of BYD. When all the orbitals involved in interactions are deleted, the conformational order is reverse of the situation when all the interactions were present, pointing out that the inversion is dictated only due to the absence of vicinal interactions. Thus, NBO results indicated that the vicinal orbital interactions play a crucial role in determining the conformational preferences in BYD.

Geminal and remote interaction deletion did not affect the energy order of gauche and trans conformers, but it caused the flipping within gauche and trans conformers. Deletion of these interactions caused an inversion in BYDA, BYDB and also in BYDC, BYDD. The relative changes in energies as a result of systematic deletions are provided in the appendix.

### 3.1.2 Experimental results

This section deals with the experimental results of the matrix isolation IR experiments of 2-Butyne-1, 4-diol. The vapor pressure of 2-Butyne-1,4-diol (sample) at room temperature is 0.0005 mm of Hg<sup>11</sup>. The sample was placed in a glass bulb (as shown in Fig. 3.6) close to the cryostat. Typically, the sample-to-matrix gas ratio used in experiments is 1:1000 to achieve isolation of the sample of interest, but in this case, the exact concentration of 2-Butyne-1, 4-diol could not be discerned to obtain a sample-to-matrix ratio. The schematic of the setup used for the deposition of the sample via the effusive beam at room temperature is given in Fig. 3.7.



**Fig. 3.6:** Glass bulb containing sample

FTIR spectra for 2-Butyne-1,4-diol using Nitrogen as the matrix gas is shown in Fig. 3.8. The matrix gas deposited through the mixing chamber gas line carried 2-butyne-1,4-diol which was kept near the KBr window. The most stable conformer BYDA is observed in the Nitrogen matrix along with the possible formation of the other two conformers, BYDB and BYDC.

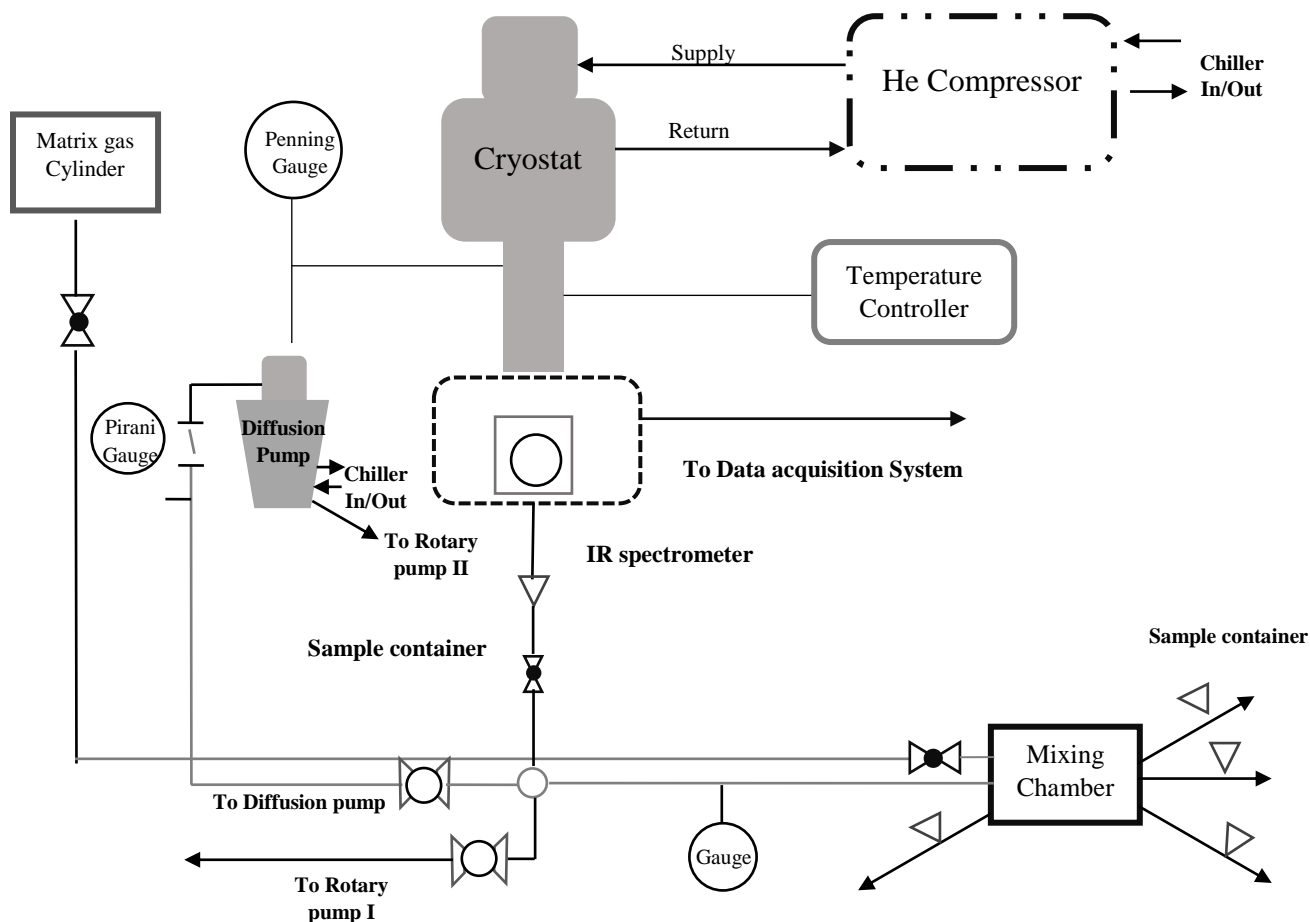


**Fig. 3.7:** Schematic of the setup used for matrix isolation FTIR experiments

The  $-OH$  stretch mode for the conformers has been shown in the spectral range of  $3660-36200\text{ cm}^{-1}$ , while the  $-CO$  stretch in the region  $1060-1000\text{ cm}^{-1}$  in the FTIR spectra. Thus, the conformational analysis of the molecule was obtained based on the identity of the characteristic  $-OH$  and  $-CO$  stretch frequency of each conformer. Fig. 3.8 shows the FTIR spectrum obtained experimentally by depositing 2-Butyne-1,4-diol at 12 K in nitrogen gas as matrix along with the simulated computed spectra using scaled frequencies obtained at MP2/aug-cc-pVDZ for various conformers. A scaling factor of 0.96, 0.98 and 0.99 was used for OH stretch, OH bent and CO stretch respectively.

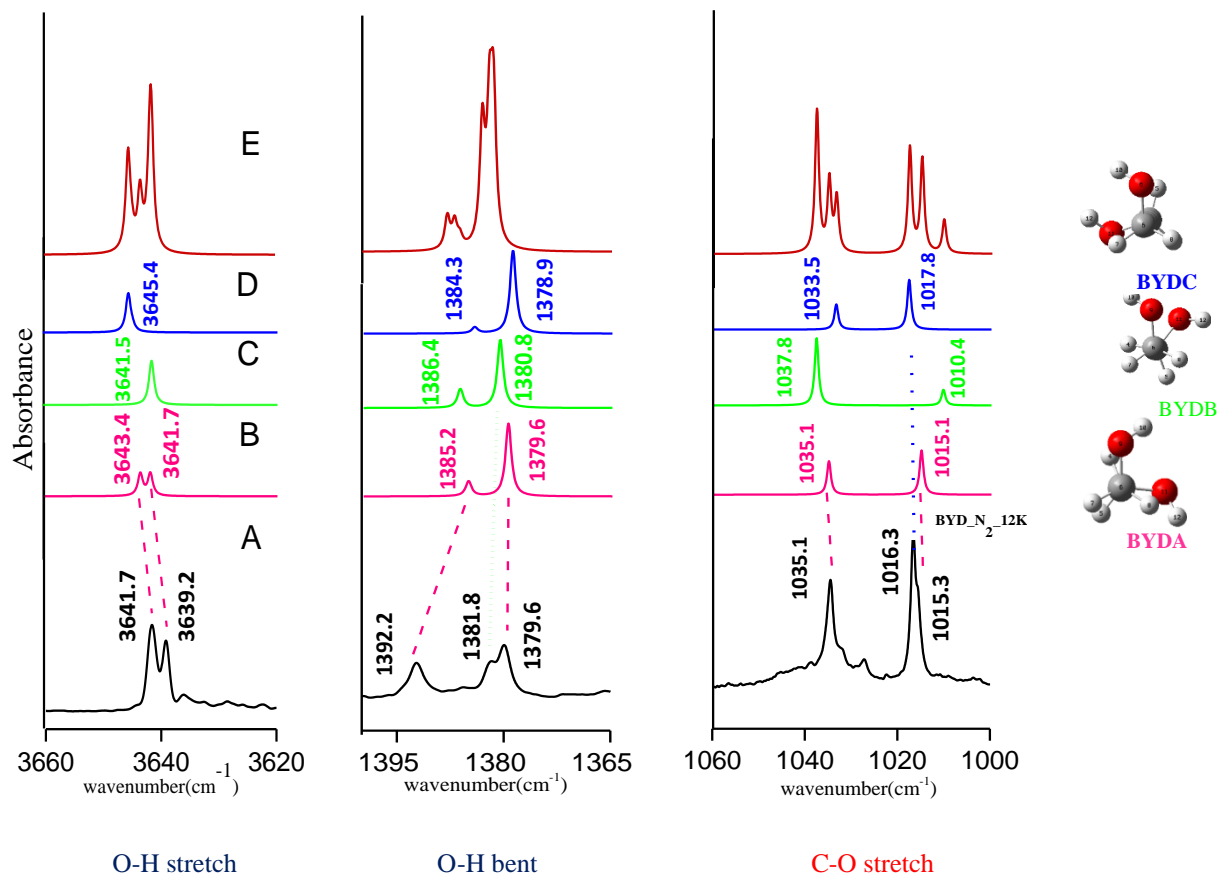


**Fig. 3.8:** A comparison between computed and experimental spectrum for 2-Butyne-1, 4-diol in  $N_2$  matrix 12K. A: Experimental Spectrum; B, C and D: Computed spectrum of BYDA, BYDB and BYDC respectively; E: Sum of the computed spectrum for all the three conformers BYDA, BYDB and BYDC.

From Fig.3.8, we can see that along with BYDA, other two lowest energy conformers BYDB and BYDC are also observed in the spectrum. The two features for BYDA corresponding to O(9)-H(10) stretch and O(11)-H(12) are seen at 3641.7 and 3639.2  $cm^{-1}$ , respectively. For BYDB the features is same at 3641.7  $cm^{-1}$ . The experiments and computations have corroborated, and the assignments are listed in Table 3.3. It is also to be noted that all the three conformers have their O-H wavenumbers very close to each other. If hydrogen bonding were to be present in any of the conformers, that particularly conformer is likely to show an O-H feature that would be red shifted relative to the other conformers where no hydrogen bonding was present. The relative proximity of the three O-H stretching in the wavenumber scale indicates that none of the conformer have intramolecular hydrogen bonding, which is consistent with our NBO and AIM analysis.

It is to be noted that the computed spectrum summed over the features corresponding to the conformers BYDA, BYDB and BYDC matches very well with the experimental spectrum indicating that all the three conformers BYDA, BYDB and BYDC are present in the matrix.

**Table 3.3:** Assignment of features (in  $\text{cm}^{-1}$ ) for BYDA in  $\text{N}_2$  matrix.\*Computed at MP2/aug-cc-pVDZ; scaled using a factor 0.96, 0.98, 0.99 for OH stretch, OH bend and CO stretch respectively.

<b>Mode assignment</b>	<b>*Computed</b>	<b>Experimental</b>
O(9)-H(10) stretch	3641.7	3639.2
O(11)-H(12) stretch	3643.4	3641.7
Symmetric OH bent coupled with CH bent	1379.6	1379.6
Anti-symmetric OH bent	1385.2	1392.2
CO anti-symmetric stretch	1015.1	1015.3
CO symmetric stretch	1035.1	1035.1

The OH bending mode was found to be coupled with the C-H bend, features for which appear at 1392.2 and 1379.6  $\text{cm}^{-1}$  in BYDA. For BYDB, the OH bent feature appears as a shoulder at 1381.8  $\text{cm}^{-1}$ . The symmetric and anti-symmetric stretch for the two C-O groups for BYDA are observed at 1035.1 and 1015.3  $\text{cm}^{-1}$  respectively. While for BYDC the anti-symmetric C-O stretch appears as a side shoulder at 1016.3  $\text{cm}^{-1}$ . From computations BYDA conformer is the most stable than BYDB and BYDC, but the population of these three low energy conformers is almost same. Thus, all three lowest energy conformers are expected to be seen in experiments as computed at the B3LYP, M06-2X and MP2 methods using aug-cc-pVDZ and 6-311++G\*\* basis sets.<sup>99</sup>

### 3.2 Interaction studies of 2-Butyne-1, 4-diol –Water Complexes

The conformational study of 2-Butyne-1, 4-diol presented in the earlier section revealed that the BYDA, BYDB, and BYDC conformers are identified in the matrix. Given the multiplicity of the BYD conformations observed experimentally, the hydrogen bonding landscape becomes rich and complicated with numerous possibilities of hydrogen-bonded isomers. In the present work, the hydrogen bonded interaction of BYD with H<sub>2</sub>O is studied to observe how the water molecule orients itself being provided with multiple hydrogen bonding sites in the BYD.

The BYDA-H<sub>2</sub>O system has been studied using *ab-initio* computations performed at HF/3-21G level of theory. Calculations have been conducted using the most stable conformer of 2-butyn-1, 4-diol, BYDA, which is unambiguously trapped in the matrix. Computations indicated that the water molecule could interact with the BYDA in several ways such as forming 1) an O-H...O interaction between the O-H group of H<sub>2</sub>O and O atom of BYD, 2) two O-H...O interactions thus forming a cyclic structure, in which both precursors serve as a proton donor and a proton acceptor simultaneously in the complex, and 3) an O-H... $\pi$  interaction between the O-H group of water and the  $\pi$  cloud of BYD. These optimized geometries for BYDA complex with water, denoted by BYDA-W are shown in Fig. 3.9. Three complexes, BYDA-W\_I, BYDA-W\_II and BYDA-W\_III are located on the potential energy surfaces as minima structures. The geometry in which water interacts with water only through an O-H... $\pi$  interaction is however not optimized at this level since such an input geometry converged to the structure bound by a strong O-H...O interaction.

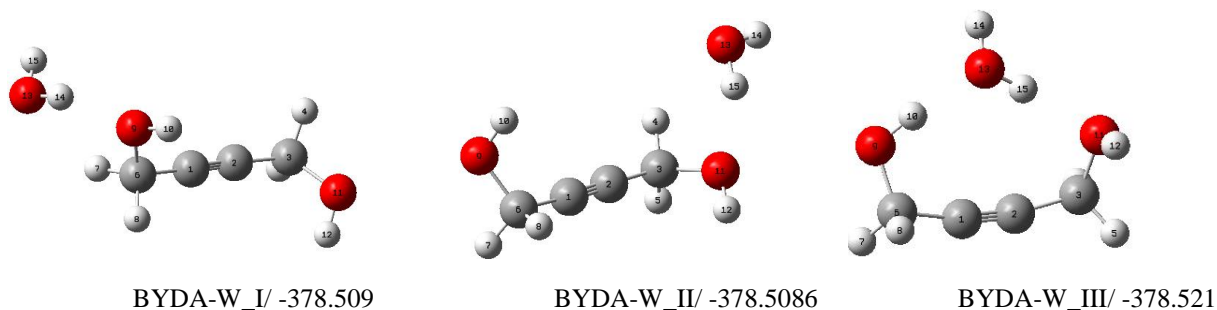


**Fig. 3.9:** Optimized structures of BYD-A complexes at HF/3-21G level of theory. Uncorrected energies in Ha

In addition to the BYDA-W\_III, complex shown in Fig. 3.9, other structures that are bounded by dual interactions are also optimized using the higher energy conformers of BYD.

These computed structures are shown in Fig. 3.10 obtained using M06-2X/aug-cc-pVDZ level of theory. In all the complexes shown in Fig. 3.10 water molecule bridges between the two hydroxyl groups of BYD, except in the case of BYDF-W', when BYDF takes a dual role with H4 as proton donor site and O9 as a proton acceptor site. The complexes BYDA-W\_III, BYDD-W, BYDE-W and, BYDF-W all have two O-H...O interactions and one O-H... $\pi$  interaction. BYDF-W' complex also shows dual interactions, but with the different binding site as now, there is a weak C-H...O interaction along with an O-H...O and an O-H...  $\pi$  interaction.

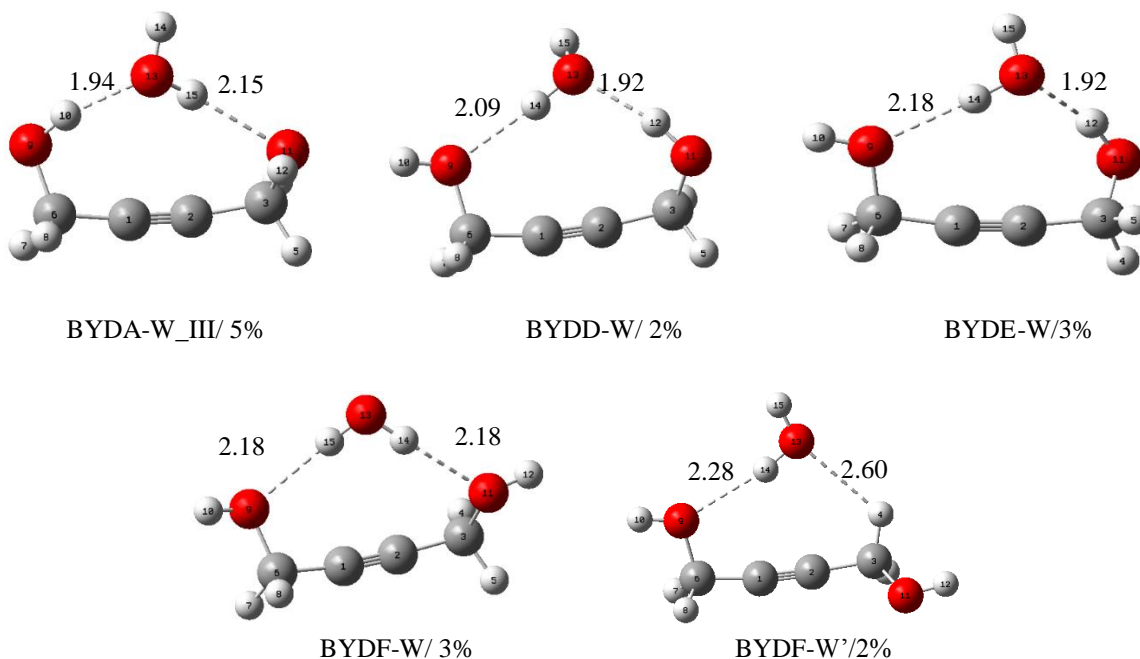


**Fig. 3.10:** Optimized structures of BYDA-W\_III and complexes of water with higher energy conformers of BYD at M06-2X/aug-cc-pVDZ level. Hydrogen bonded distances have been shown as dotted lines with bond distances in Å units. Change in linearity of C-C-C-C backbone is given in %

We also see that complexation of 2-butyne-1,4-diol with water causes a change in the linearity of C6-C1-C2-C3 backbone in 2-butyne-1,4-diol. The amount of change in linearity is expressed in the form of a percentage along with the complexes in Fig.3.10. Complexes for BYDB and BYDC could not be optimized; it was seen that the BYDB, BYDC flipped into other higher energy conformers. The interaction energy values for optimized BYD-W complexes computed at M06-2X/aug-cc-pVDZ level are given in Table 3.4.

**Table 3.4:** Interaction energies for 2-butynediol complexes

Complex	Interaction Energy(in kcal/mol)
	Raw/ZPCE/BSSE
BYDA-W_III	9.6/7.0/9.1
BYDD- W	10.2/7.9/9.8
BYDE-W	10.7/8.3/10.2
BYDF-W	7.6/5.3/7.2
BYDF-W'	6.2/4.5/5.7

From table 3.4, the BYDE-W complex is the most stable complex and not the BYDA-W\_III. This could be reasoned from Fig. 3.12, correlation diagram showing the relative locations of BYD-W complexes on the energy axis computed at M06-2X/aug-cc-pVDZ level. In this figure, each complex was correlated with the monomer asymptote to which that particular complex correlates. It can be seen from the figure that BYDE-W is more stable than BYDA-W\_III complex, this is because the monomer asymptote of BYDE-W is located at higher energy compared to the BYDA-W\_III. However, BYDE-W has higher interaction energy; it correlates with higher energy monomer asymptote, thus it is unlikely to be seen in experiments.

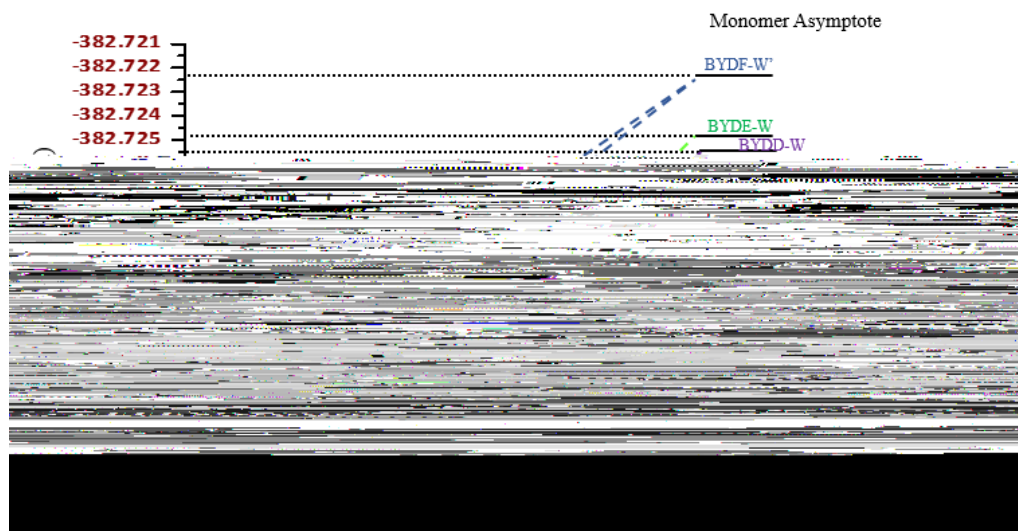


**Fig. 3.11:** Correlation diagram to show the relative locations of BYD-W complexes on the energy axis. The difference in energy between the monomer asymptote and the complexes corresponds to uncorrected interaction energy (Ha) at M06-2X/aug-cc-pVDZ level. The plotted energy levels are to scale on the energy axis.

The presence of these intermolecular hydrogen bonds was verified by AIM analysis, as shown in Fig. 3.11. The bond critical points and ring critical point has been shown. It is found that together with the dual interactions mentioned above, an O-H... $\pi$  interaction is also present in these geometries with water interacting with the acetylenic  $\pi$ -cloud of BYD. No intramolecular hydrogen bonding in 2-butynediol is seen via AIM analysis even when it forms complex with water.

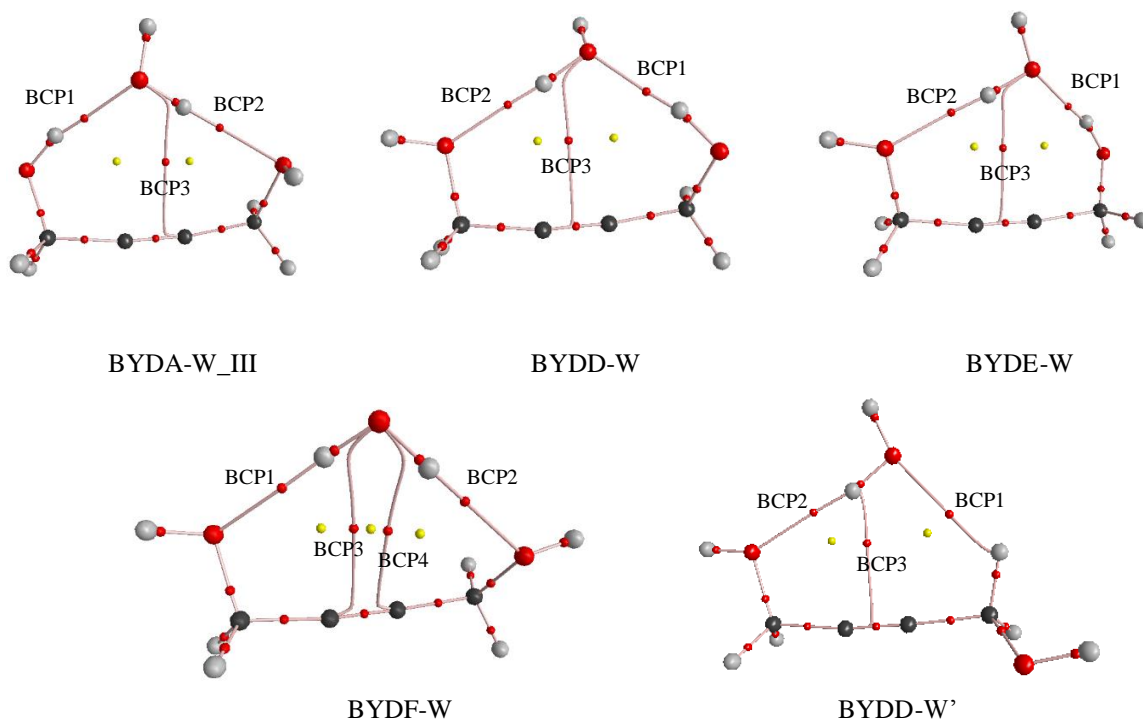


**Fig. 3.12:** AIM analysis of BYD-W complexes

The method provided by Espinosa et al.<sup>40</sup> using the topological analysis of electron densities by AIM analysis was used to quantitatively decipher the inter-molecular hydrogen bond strengths of different hydrogen bonding interactions involved. The topological criteria for the existence of hydrogen bond are that the electron density value at the H-X (BCP) should be in the range of 0.002-0.034 a.u., whereas the Laplacian value within 0.024-0.139 a.u. The values of electron density, Laplacian at BCP for the complexes are shown in Table 3.5.

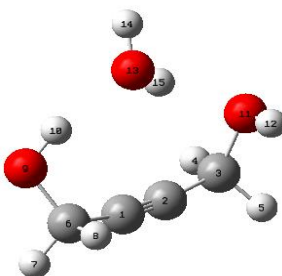
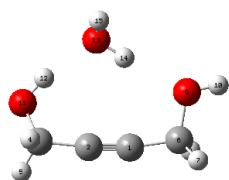
**Table 3.5:** AIM analysis of BYDA-W\_III, BYDD-W, BYDE-W, BYDF-W and BYDF-W' complexes

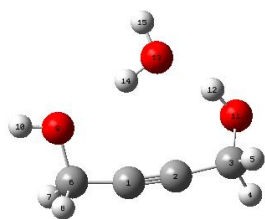
Complex	$\rho(r_c)$	Laplacian	$\lambda_1$	$\lambda_2$	$\lambda_3$	$\lambda_1/\lambda_3$	$[\lambda_1/\lambda_2]-1$
<b>BYDA-W_III</b>							
BCP1/O-H...O	0.024	0.090	-0.03045	-0.02867	0.14918	-0.20413	0.06218
BCP2/O...H-O	0.016	0.051	-0.01779	-0.01744	0.08599	-0.20691	0.02026
BCP3/ $\pi$ ...OH	0.009	0.032	-0.00658	-0.00232	0.04089	-0.16086	1.82942
<b>BYDD-W</b>							
BCP1/O-H...O	0.0252	-0.024	-0.03293	-0.03166	0.16077	-0.20481	0.03992
BCP2/O...H-O	0.0161	-0.0147	-0.01798	-0.01712	0.09393	-0.1914	0.0499
BCP3/ $\pi$ ...OH	0.0087	-0.0076	-0.0066	-0.00195	0.03912	-0.16874	2.39235
<b>BYDE-W</b>							
BCP1/O-H...O	0.0246	-0.0238	-0.03209	-0.03018	0.15745	-0.20381	0.06328
BCP2/O...H-O	0.0149	-0.0135	-0.01625	-0.01535	0.08562	-0.18979	0.05884
BCP3/ $\pi$ -OH	0.0092	-0.0083	-0.00693	-0.00266	0.0427	-0.16232	1.60214
<b>BYDF-W</b>							
BCP1/O...H-O	0.0139	-0.0116	-0.01488	-0.0141	0.07533	-0.19759	0.05541
BCP2/O...H-O	0.0138	-0.0116	-0.01484	-0.01406	0.07511	-0.19752	0.05554
BCP3/ $\pi$ -OH	0.0073	-0.0063	-0.00496	-0.00105	0.03108	-0.15963	3.74541
BCP4/ $\pi$ -OH	0.0073	-0.0063	-0.00496	-0.00105	0.03107	-0.15967	3.74016
<b>BYDF-W'</b>							
BCP1/C-H...O	0.0072	-0.0067	-0.00636	-0.00499	0.03808	-0.16710	0.27626
BCP2/O...H-O	0.0107	-0.0089	-0.0102	-0.01009	0.05594	-0.18240	0.01161
BCP3/ $\pi$ -OH	0.0100	-0.0085	-0.00794	-0.00466	0.04665	-0.17024	0.70459

NBO analysis was also performed to understand the orbital interactions involved in H-bonded complexes BYDA-W\_III, BYDD-W, BYDE-W, BYDF-W, and BYDF-W' at M06-2X/aug-cc-pVDZ level. The activity of lone pair of O atom in H<sub>2</sub>O, OH group of 2-butyne-1, 4-diol and the acetylenic  $\pi$ -cloud plays a crucial role in these interactions. The presence of inter-

molecular hydrogen bonds for which the bond critical points were located in AIM analysis can also be confirmed through NBO analysis in terms of the orbital interactions.

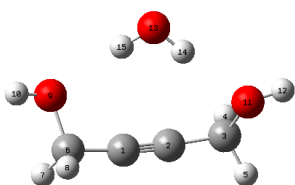
**Table 3.7:** NBO analysis of BYDA-W\_III, BYDD-W, BYDE-W, BYDF-W and BYDFW' complexes

Conformation	Donor NBO(i)	Acceptor NBO(j)	E(2)	E(j)-E(i)	F(i, j)
			[kcal/mol]	[ a.u.]	[a.u.]
 BYDA-W_III	BD C(1)-C(2)	$\sigma^*$ O(13)-H(14)	0.14	0.89	0.010
	BD C(1)-C(2)	$\sigma^*$ O(13)-H(15)	0.41	0.88	0.017
	BD O(9)-H(10)	$\sigma^*$ O(13)-H(14)	0.09	1.34	0.010
	BD O(11)-H(12)	$\sigma^*$ O(13)-H(15)	0.06	1.36	0.008
	LP1 O(11)	$\sigma^*$ O(13)-H(15)	0.80	1.27	0.028
	LP2 O(11)	$\sigma^*$ O(13)-H(15)	3.85	0.94	0.054
	BD O(13)-H(15)	$\sigma^*$ O(9)-H(10)	0.09	1.39	0.010
	LP2 O(13)	$\pi^*$ C(1)-C(2)	0.18	0.80	0.011
	LP1 O(13)	$\sigma^*$ O(9)-H(10)	0.18	1.06	0.013
	LP2 O(13)	$\sigma^*$ O(9)-H(10)	11.24	1.16	0.102
 BYDD-W	BD C(1)-C(2)	$\sigma^*$ O(13)-H(14)	0.44	0.88	0.018
	BD O(11)-H(12)	$\sigma^*$ O(13)-H(15)	0.08	1.34	0.009
	LP1 O(9)	$\sigma^*$ O(13)-H(14)	3.15	1.26	0.056
	LP2 O(9)	$\sigma^*$ O(13)-H(14)	1.34	0.97	0.032
	BD O(13)-H(14)	$\sigma^*$ O(9)-H(10)	0.08	1.33	0.009
	BD O(13)-H(14)	$\sigma^*$ O(11)-H(12)	0.11	1.38	0.011
	LP1 O(13)	$\sigma^*$ O(11)-H(12)	0.36	1.08	0.018
	LP2 O(13)	$\pi^*$ C(1)-C(2)	0.20	0.78	0.011
	LP2 O(13)	$\sigma^*$ C(6)-O(9)	0.05	0.91	0.006
	LP2 O(13)	$\sigma^*$ O(11)-H(12)	12.55	1.14	0.107



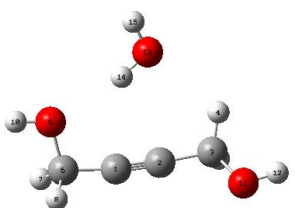
BYDE-W

BD C(1)-C(2)	$\sigma^*$ O(13)-H(14)	0.47	0.89	0.018
BD C(1)-C(2)	$\sigma^*$ O(13)-H(15)	0.13	0.90	0.010
BD O(9)-H(10)	$\sigma^*$ O(13)-H(14)	0.06	1.37	0.008
BD O(11)-H(12)	$\sigma^*$ O(13)-H(15)	0.13	1.34	0.012
LP1 O(9)	$\sigma^*$ O(13)-H(14)	3.43	1.28	0.059
LP2 O(9)	$\sigma^*$ O(13)-H(14)	0.07	0.96	0.007
LP1 O(11)	$\sigma^*$ O(13)-H(15)	0.05	1.21	0.007
BD O(13)-H(14)	$\sigma^*$ O(9)-H(10)	0.09	1.33	0.010
BD O(13)-H(14)	$\sigma^*$ O(11)-H(12)	0.09	1.38	0.010
LP1 O(13)	$\sigma^*$ O(11)-H(12)	0.13	1.03	0.010
LP2 O(13)	$\pi^*$ C(1)-C(2)	0.23	0.83	0.012
LP2 O(13)	$\sigma^*$ O(11)-H(12)	11.66	1.19	0.105



BYDF-W

BD C(1)-C(2)	$\sigma^*$ O(13)-H(14)	0.19	0.95	0.012
BD C(1)-C(2)	$\sigma^*$ O(13)-H(15)	0.19	0.95	0.012
LP1 O(9)	$\sigma^*$ O(13)-H(15)	1.35	1.31	0.038
LP2 O(9)	$\sigma^*$ O(13)-H(14)	1.58	1.01	0.036
LP2 O(11)	$\sigma^*$ O(13)-H(15)	1.36	1.31	0.038
LP2 O(11)	$\sigma^*$ O(13)-H(14)	1.56	1.01	0.036
BD O(13)-H(14)	$\pi^*$ C(1)-C(2)	0.06	0.97	0.007
BD O(13)-H(15)	$\pi^*$ C(1)-C(2)	0.07	0.97	0.007



BYDF-W'

BD2 C(1)-C(2)	$\sigma^*$ O(13)-H(14)	0.09	0.91	0.008
BD3 C(1)-C(2)	$\sigma^*$ O(13)-H(14)	0.63	0.91	0.022
BD3 C(1)-C(2)	$\sigma^*$ O(13)-H(15)	0.10	0.91	0.009
BD O(9)-H(10)	$\sigma^*$ O(13)-H(14)	0.06	1.38	0.010
LP1 O(9)	$\sigma^*$ O(13)-H(14)	1.55	1.30	0.040
LP1 O(13)	$\pi^*$ C(1)-C(2)	0.14	0.72	0.009
LP2 O(13)	$\pi^*$ C(1)-C(2)	0.21	0.75	0.011
LP1 O(13)	$\sigma^*$ C(1)-H(4)	0.35	1.02	0.017
LP2 O(13)	$\sigma^*$ C(1)-H(4)	0.73	1.05	0.025

In BYDA-W\_III, water molecule complexes with BYDA through three interactions as revealed from AIM analysis. The lone pairs of O11 atom in BYD donate electrons into  $\sigma^*$  (anti-bonding) orbital of O13-H15 of water. Another delocalization can be seen in between the lone pair of water O13 and the  $\sigma^*$  (anti-bonding) of O9-H10 bond in 2-butyne-1,4-diol. There is also a weak contribution from the acetylenic  $\pi$ -cloud of BYD to the O13-H15 of water with second-order perturbation energy,  $E(2)$  of 0.41 kcal/mol.

Similarly, for BYDD-W, BYDE-W we see two O-H...O interactions along with weaker  $\pi \dots \sigma^*$ O13-H14 interactions. However, an interesting case is BYDF, where water can complex in two geometries one is stabilized by two O-H...O interactions and two weak  $\pi \dots \sigma^*$ O13-H14,  $\pi \dots \sigma^*$ O13-H15 interactions while in other geometry it changes the geometry of BYD to form a slightly higher in energy C-H...O interaction along with the one O-H...O and  $\pi \dots \sigma^*$ O13-H14 interaction. Thus, even though the higher energy conformers of BYD have high interaction energies on forming complex with water, they are not expected to be seen in experiments.

## Chapter 4

### Conclusion

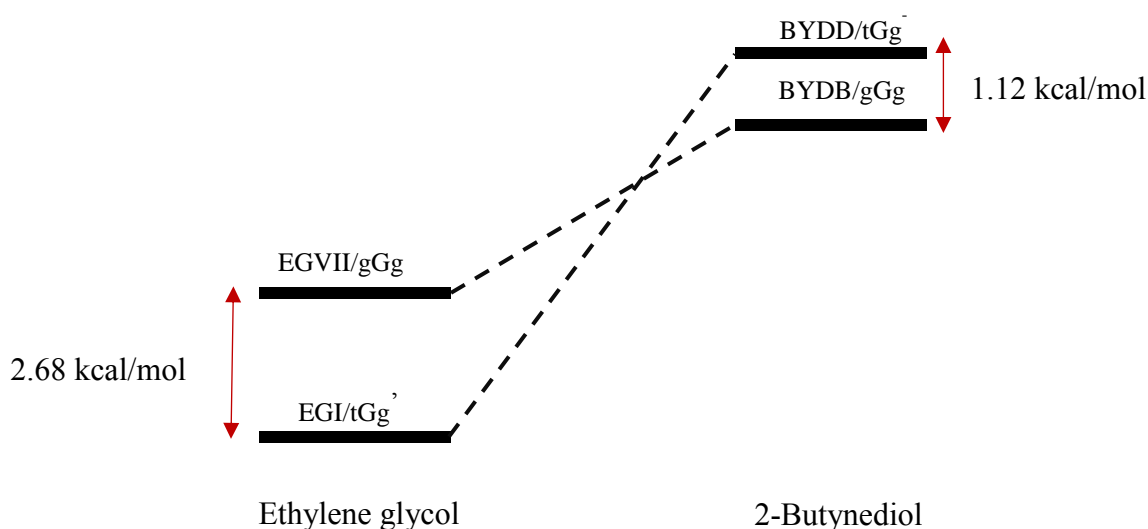
Matrix Isolation infrared spectroscopy which is a powerful tool to study weak interactions and conformers was used in the conformational analysis of 2-butyne-1,4-diol in combination with the *ab-initio* computational study. Geometry optimization of 2-Butyne-1,4-diol was done at various levels of theory such as the B3LYP, M06-2X, and MP2 together with 6-311++G\*\* and aug-cc-pVDZ basis sets.

The conformational analysis yielded six different stable conformers computationally, while the experiments show the presence of the lowest energy conformer and possibly two other isoenergetic structures in the nitrogen matrix. These have been labelled as BYDA(gGg), BYDB(gGg) and BYDC(gGg) conformers. Experiments show the presence of three lowest energy conformers of BYD.

#### 4.1 Influence of acetylenic $\pi$ -cloud

Starting with the two stable (g-PA, t-PA) conformers in propargyl alcohol and ten stable conformers in ethylene glycol, we have computed six stable conformers for 2-Butyne-1,4-diol. Previous studies on propargyl alcohol<sup>10</sup> found two conformers g-PA, t-PA. The gauche conformer was found to be more stable compared to the trans conformer in the PA system. Similarly, earlier work on ethylene glycol<sup>41,42</sup> reports ten optimized structures which suggest the stability of trans over gauche conformer. The conformational stability order of ethylene glycol is found to be reversed in the 2-Butyne-1,4-diol system as shown in Fig. 4.1. Thus, a comparative study of PA and EG system with 2-Butynediol presents us with an interesting possibility of the acetylenic moiety affecting the energy ordering of these conformers.

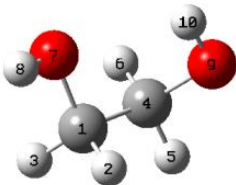
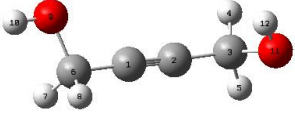
The data on ethylene glycol has been taken from Ref.41 for comparison. The introduction of the acetylenic spacer in between the two diols causes a flip in the energy ordering of the ethylene glycol system. The relative energy difference between the trans and gauche of EG decreases up to ~1.12 kcal/mol because of the presence of the acetylenic moiety. Further, this switching of tGg' (EGI) and gGg (EGVII) in 2-butyne-1,4-diol can be explored through the NBO analysis.



**Fig. 4.1:** Ethylene glycol compared with 2-Butynediol

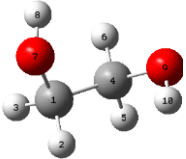
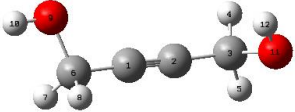
NBO analysis of EGI and BYDD provided in Table 4.1 suggests that the weak O $\cdots$ H-O interaction is the reason for the stability of EGI which is diminished in BYDD due to the presence of a spacer in between two diol. The LP O(7) can be donated to anti-bonding of O(9)-H(10) in ethylene glycol, but with an acetylenic group in between, the distance of two between OH groups increases and decreases the possibility of any intramolecular hydrogen bonding interaction between the two O-H groups.

**Table 3.1:** NBO analysis of ethylene glycol, EGI(tGg') and 2-butynediol, BYDD(tGg')

Conformation	Donor NBO(i)	Acceptor NBO(j)	E(2)	E(j)-E(i)	F(i, j)
			[Kcal/mol]	[ a.u.]	[a.u.]
 EGI(tGg')	LP1 O(7)	$\sigma^*C(1)-H(2)$	2.43	1.52	0.05
	LP2 O(7)	$\sigma^*C(1)-H(2)$	5.02	1.16	0.07
	LP2 O(7)	$\sigma^*C(1)-H(3)$	9.59	1.16	0.09
	LP2 O(7)	$\sigma^*O(9)-H(10)$	0.64	1.24	0.02
	LP1 O(9)	$\sigma^*C(4)-H(5)$	2.28	1.52	0.05
	LP2 O(9)	$\sigma^*C(1)-C(4)$	5.75	1.13	0.07
	LP2 O(9)	$\sigma^*C(4)-H(6)$	9.24	1.14	0.09
 BYDD(tGg')	LP1 O(9)	$\sigma^*C(1)-C(6)$	11.32	1.60	0.041
	LP1 O(9)	$\sigma^*C(6)-H(7)$	1.06	1.53	0.036
	LP2 O(9)	$\sigma^*C(6)-H(7)$	7.61	1.15	0.084
	LP1 O(9)	$\sigma^*C(6)-H(8)$	1.11	1.53	0.037
	LP2 O(9)	$\sigma^*C(6)-H(8)$	7.49	1.15	0.083
	LP1 O(11)	$\sigma^*C(2)-C(3)$	1.51	1.57	0.044
	LP2 O(11)	$\sigma^*C(2)-C(3)$	7.44	1.22	0.085
	LP1 O(11)	$\sigma^*C(3)-H(4)$	1.57	1.52	0.044
	LP2 O(11)	$\sigma^*C(3)-H(4)$	7.65	1.16	0.084
	LP1 O(11)	$\sigma^*C(3)-H(5)$	2.50	1.52	0.055
LP2 O(11)	$\pi^*C(1)-C(2)$	0.90	0.83	0.024	

On comparing the NBO of EGVII and BYDB system as provided in Table 4.2, we see that the contribution of O(9) and O(11) to the anti-bonding orbital of acetylenic  $\pi$ -cloud of C(1)-C(2) is of ~1 kcal/mol which is absent in EGVII could be the reason for the stabilization of EGVII(gGg) in BYD.

**Table 4.2:** NBO analysis of ethylene glycol, EGVII (gGg) and 2-butynediol, BYDB(gGg)

Conformation	Donor NBO(i)	Acceptor NBO(j)	E(2)	E(j)-E(i)	F(i, j)
			[kcal/mol]	[ a.u.]	[a.u.]
 EGVII(gGg)	LP2 O(7)	$\sigma^*C(1)-H(3)$	10.40	1.14	0.10
	LP2 O(7)	$\sigma^*C(1)-C(4)$	5.18	1.14	0.07
	LP1 O(9)	$\sigma^*C(1)-C(4)$	5.18	1.14	0.07
	LP2 O(9)	$\sigma^*C(4)-H(6)$	10.40	1.14	0.10
 BYDB(gGg)	LP1 O(9)	$\sigma^*C(1)-C(6)$	1.59	1.57	0.045
	LP2 O(9)	$\sigma^*C(1)-C(6)$	7.33	1.22	0.084
	LP1 O(9)	$\sigma^*C(6)-H(7)$	1.52	1.51	0.043
	LP1 O(9)	$\sigma^*C(6)-H(7)$	7.85	1.16	0.085
	LP2 O(9)	$\sigma^*C(6)-H(8)$	2.53	1.52	0.056
	LP2 O(9)	$\pi^*C(1)-C(2)$	1.04	0.83	0.026
	LP1 O(11)	$\sigma^*C(2)-C(3)$	1.59	1.57	0.045
	LP2 O(11)	$\sigma^*C(2)-C(3)$	7.33	1.22	0.084
	LP1 O(11)	$\sigma^*C(3)-H(4)$	2.53	1.52	0.056
	LP1 O(11)	$\sigma^*C(3)-H(5)$	1.52	1.51	0.043
	LP2 O(11)	$\sigma^*C(3)-H(5)$	7.85	1.16	0.085
	LP2 O(11)	$\pi^*C(1)-C(2)$	1.04	0.83	0.026

Effect of acetylenic moiety can also be substantiated by comparing the BYD system with propargyl alcohol. We see that when a hydroxymethyl group is added to the PA system the energy ordering and the relative energy difference between the gauche and trans conformer does not change.

Thus it can be clearly stated that the introduction of an alkyl group in a vicinal diol system perturbs the system heavily and changes the stability order of conformers.

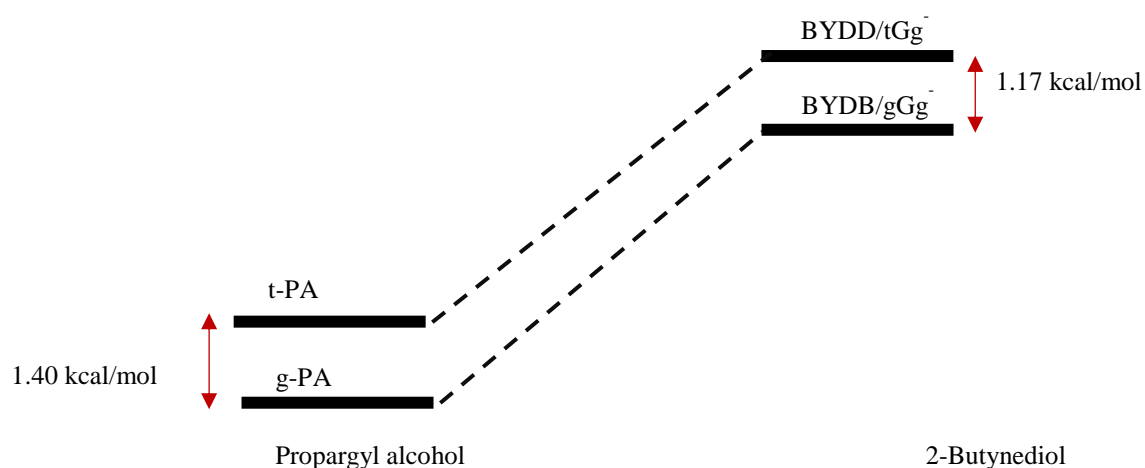


**Fig. 4.2:** Comparison of Propargyl alcohol and 2-butynediol

#### BYD-Water system

BYD-W system is of special interest from the hydrogen bonding point of view as the multiple possibilities for proton donating and accepting sites exist. For BYD-water complexes, the *ab initio* study on BYDA-W complexes yielded three optimized geometries at HF/3-21G. While for all the six conformers of BYD, water can complex in such a way that it tries to form more number of hydrogen bonding interactions. Complexes, where water bridges itself through the two OHs of BYD were studied at M06-2X/aug-cc-pVDZ level of theory. Zero point corrected, Basis set superposition error corrected energy values were calculated for all these complexes. These complexes were then further studied through NBO and AIM analysis. BYDF presents a compelling case as it can bridge with water through O-H...O interactions and weaker O-H... $\pi$  interactions while in another case BYDF-W' it can form O-H...O and a C-H...O interaction. We also observed that when BYD and H<sub>2</sub>O form a complex 2-butynediol submolecule becomes slightly non-linear in all of the complexes. This deviation in linearity can be accounted by the formation of strong hydrogen bonding interactions and a consequent change in the hybridization of the carbon atoms of the diol.

## 4.2 Future Scope

The effect of matrix on conformational stability can be studied if the conformers observed in Nitrogen matrix are also found in Argon matrix and also the effect of annealing on the conformers.

With no previous work on 2-butyne-1,4-diol or BYD and BYD-W system needs to be investigated through *ab initio* calculations and matrix –isolation experiments. Computations at HF level have been done for BYDA-W complex, and these can be used to perform computations at a higher level. BYDA-W complexes should be studied at higher levels of theory and at higher basis sets. Matrix Isolation IR spectroscopy, along with the ab-initio computational study needs to be performed to investigate the BYD-W system.

## Bibliography

- (1) Arunan, E.; Desiraju, G. R.; Klein, R. A.; Sadlej, J.; Scheiner, S.; Alkorta, I.; Clary, D. C.; Crabtree, R. H.; Dannenberg, J. J.; Hobza, P.; et al. Definition of the Hydrogen Bond ( IUPAC Recommendations 2011 )\*. *pure* **2011**, 83 (8), 1637–1641.
- (2) Desiraju, G. R. C–H···O and Other Weak Hydrogen Bonds. From Crystal Engineering to Virtual Screening. *Chem. Commun.* **2005**, No. 24, 2995–3001.
- (3) J.A., Jeffery , Saenger, W. Hydrogen Bonding in Biological Structures; Springer-Verlag. <https://doi.org/10.1007/978-3-642-85135-3>.
- (4) Moore, T. S.; Winmill, T. F. CLXXVII.—The State of Amines in Aqueous Solution. *J. Chem. Soc. Trans.* **1912**, 101 (0), 1635–1676. (5) Latimer, W. M.; Rodebush, W. H. POLARITY AND IONIZATION FROM THE STANDPOINT OF THE LEWIS THEORY OF VALENCE. *J. Am. Chem. Soc.* **1920**, 42 (7), 1419–1433. <https://doi.org/10.1021/ja01452a015>.
- (6) Cubero, E.; Orozco, M.; Hobza, P.; Luque, F. J. Hydrogen Bond versus Anti-Hydrogen Bond: A Comparative Analysis Based on the Electron Density Topology. *J. Phys. Chem. A* **1999**, 103 (32), 6394–6401.
- (7) Arunan, E.; Desiraju, G. R.; Kline, R. A.; Sadlej, J.; Schreiner, S.; Alkorta, I.; Clary, D.C.; Crabtree, R.H.; Dannenberg, J. J.; Hobza, P.; Kjaergaard, H. G.; Legon, A. C.; Mennucci B.; Nesbitt, D. J. Defination of Hydrogen Bond (IUPAC Recommendations). *Pure. Appl. Chem.* **2011**, 83, 1637–1641.
- (8) Perlstein, J. The Weak Hydrogen Bond In Structural Chemistry and Biology (International Union of Crystallography, Monographs on Crystallography, 9) By Gautam R. Desiraju (University of Hyderabad) and Thomas Steiner (Freie Universität Berlin). Oxford University Press: . *J. Am. Chem. Soc.* **2001**, 123 (1), 191–192.
- (9) Scheiner, S. Weak H-Bonds. Comparisons of CH···O to NH···O in Proteins and PH···N to Direct P···N Interactions. *Phys. Chem. Chem. Phys.* **2011**, 13 (31), 13860–13872.

- (10) Saini, J.; Viswanathan, K. S. Does a Hydrogen Bonded Complex with Dual Contacts Show Synergism? A Matrix Isolation Infrared and Ab-Initio Study of Propargyl Alcohol–Water Complex. *J. Mol. Struct.* **2016**, *1118*, 147–156.
- (11) [https://pubchem.ncbi.nlm.nih.gov/compound/2-Butyne-1\\_4-diol](https://pubchem.ncbi.nlm.nih.gov/compound/2-Butyne-1_4-diol).
- (12) Whittle, E.; Dows, D. A.; Pimentel, G. C. Matrix Isolation Method for the Experimental Study of Unstable Species. *J. Chem. Phys.* **1954**, *22* (11), 1943. <https://doi.org/10.1063/1.1739957>.
- (13) Norman, I.; Porter, G. Trapped Atoms and Radicals in a Glass ‘Cage.’ *Nature* **1954**, No. 174, 508–509.
- (14) Thomas, B. Matrix Isolation. In *Reactive Intermediate Chemistry*; Moss Robert A., Plat Matthew S.z, and Maitland Jones, J., Ed.; Fribourg.
- (15) Goswami, M.; Arunan, E. Microwave Spectroscopic and Theoretical Studies on the Phenylacetylene···H<sub>2</sub>O Complex: C–H···O and O–H··· $\pi$  Hydrogen Bonds as Equal Partners. *Phys. Chem. Chem. Phys.* **2011**, *13*, 14153–14162.
- (16) Sander, W.; Costa, P. Hydrogen Bonding Switches the Spin State of Diphenylcarbene from Triplet to Singlet. *Angew. Chem. Int. Ed.* **2014**, *53*, 1–5.
- (17) Hobe, M. von; Stroh, F.; Beckers, H.; Benter, T.; Willner, H. The UV/Vis Absorption Spectrum of Matrix-Isolated Dichlorine Peroxide, ClOOC<sub>l</sub>. *Phys. Chem. Chem. Phys.* **2009**, *11*, 1571–1580.
- (18) Sander, W.; Bucher, G.; Wierlacher, S. Carbenes in Matrixes: Spectroscopy, Structure, and Reactivity. *Chem. Rev.* **1993**, *93* (4), 1583–1621.
- (19) Ferrante, R. F. Spectroscopy of Matrix-isolated Methylnitrene. *J. Chem. Phys.* **1987**, *86* (1), 25–32.
- (20) Bahou, M. . D. P. . L. Y. P. Infrared Spectra of Free Radicals and Protonated Species Produced in Para-Hydrogen Matrices. *Phys. Chem. Chem. Phys.* **2014**, *16*, 2200.
- (21) Press W., Janik B., G. H. ,49, 9-161. *Phys-B Condens. matter* **1982**, *49*, 9–16.
- (22) A.J., B. Vibrational Spectroscopy of Hydrogen Halide Molecular Complexes Trapped in Low-Temperature Matrices. *J. Mol. Struct.* **1980**, *60*, 343–346.
- (23) Pimental, G. ; Charles, S. Infrared Spectral Perturbations in Matrix Experiments. *Pure Appl.*

- Chem.* **2009**, 7 (1), 111–124.
- (24) Nelander, B. An FTIR Study of the Rotation of Ammonia in Solid Nitrogen. *Chem. Phys.* **1984**, 87 (2), 283–294.
- (25) Nelander, B. An FTIR Study of the Rotation of Ammonia in Solid Nitrogen. *Chem. Phys.* **1984**, 87 (2), 283–294.
- (26) Robinson, D. W. Spectra of Matrix-Isolated Water in the "Pure Rotation" Region. *J. Chem. Phys.* **1963**, 39 (12), 3430–3432.
- (27) Bowers, M. T.; Kerley, G. I.; Flygare, W. H. Vibration—Rotation Spectra of Monomeric HF in the Rare-Gas Lattices. II. *J. Chem. Phys.* **1966**, 45 (9), 3399–3414.
- (28) Lee, Y.-P.; Wu, Y.-J.; Lees, R. M.; Xu, L.-H.; Hougen, J. T. Internal Rotation and Spin Conversion of CH<sub>3</sub>OH in Solid Para-Hydrogen. *Science* **2006**, 311 (5759), 365–368.
- (29) M. J. Frisch, G. W. Trucks, H. B. Schlegel, G. E. S. et. al. Gaussian 09. Wallingford, CT 2009.
- (30) Calais, J.-L. Density-Functional Theory of Atoms and Molecules. R.G. Parr and W. Yang, Oxford University Press, New York, Oxford, 1989. IX + 333 Pp. Price £45.00. *Int. J. Quantum Chem.* **1993**, 47 (1), 101.
- (31) K., I. *The Spectra Were Simulated Using SYNSPEC Made Available By*; Gaithersburg, MD 20899, USA, 1995.
- (32) Boys, S. F.; Bernardi, F. The Calculation of Small Molecular Interactions by the Differences of Separate Total Energies. Some Procedures with Reduced Errors. *Mol. Phys.* **1970**, 19 (4), 553–566.
- (33) Helgaker, T.; Klopper, W.; Koch, H.; Noga, J. Basis-Set Convergence of Correlated Calculations on Water. *J. Chem. Phys.* **1997**, 106 (23), 9639–9646.
- (34) KUMAR, P. S. V.; RAGHAVENDRA, V.; SUBRAMANIAN, V. Bader's Theory of Atoms in Molecules (AIM) and Its Applications to Chemical Bonding. *J. Chem. Sci.* **2016**, 128 (10), 1527–1536.
- (35) Biegler-König, F.; Schönbohm, J. Update of the AIM2000-Program for Atoms in Molecules. *J. Comput. Chem.* **2002**, 23 (15), 1489–1494.

- (36) Koch, U.; Popelier, P. L. A. Characterization of C-H-O Hydrogen Bonds on the Basis of the Charge Density. *J. Phys. Chem.* **1995**, *99* (24), 9747–9754.
- (37) Su, P.; Li, H. Energy Decomposition Analysis of Covalent Bonds and Intermolecular Interactions. *J. Chem. Phys.* **2009**, *131* (1), 14102..
- (38) Glendening, E. D.; Carpenter, J. E.; Weinhold, F. NBO. Pittsburgh 2003.
- (39) Radom, L.; A. Lathan, W.; J. Hehre, W.; A. Pople, J. *Molecular Orbital Theory of the Electronic Structure of Organic Compounds. XVII. Internal Rotation in 1,2-Disubstituted Ethanes*; 1973; Vol. 95. <https://doi.org/10.1021/ja00784a008>.
- (40) Espinosa, E.; Molins, E.; Lecomte, C. *Hydrogen Bond Strengths Revealed by Topological Analyses of Experimentally Observed Electron Densities*; 1998; Vol. 285. [https://doi.org/10.1016/S0009-2614\(98\)00036-0](https://doi.org/10.1016/S0009-2614(98)00036-0).
- (41) Gupta, D. A Matrix Isolation -FTIR and Ab Initio Study of Ethylene Glycol :Conformations and Hydrogen Bonded Complexes, Indian Institute of Science Education& Research(IISER)-Mohali, 2018. <https://doi.org/April,20,2018>.
- (42) Cramer, C. J.; Truhlar, D. G. Quantum Chemical Conformational Analysis of 1,2-Ethenediol: Correlation and Solvation Effects on the Tendency To Form Internal Hydrogen Bonds in the Gas Phase and in Aqueous Solution. *J. Am. Chem. Soc.* **1994**, *116* (9), 3892–3900.

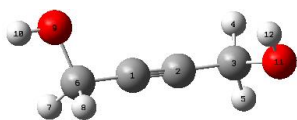
## Appendix

**Table 1:** Dihedral Angles of 2-Butynediol conformers

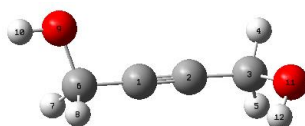
Conformer	Notation	Dihedral Angle (H10-O9-C6-C1)	Dihedral Angle (O9-C6-C3-O1)	Dihedral Angle (H12-O11-C3-C2)
BYDA	g <sup>-</sup> Gg (A)	-53	-96	51
BYDB	gGg (B)	50	40	50
BYDC	gG <sup>-</sup> g (C)	52	-108	52
BYDD	tGg <sup>-</sup> (D)	180	-91	51
BYDE	tGg (E)	180	94	50
BYDF	tTt (F)	-179	103	-179

**Table 3:** NBO Analysis for 2-Butynediol conformations BYDD-BYDE

Conformation	Donor NBO(i)	Acceptor NBO(j)	E(2) [Kcal/mol]	E(j)-E(i) [ a.u.]	F(i, j) [a.u.]
BYDD	LP1 O(9)	$\sigma^*$ C(1)-C(6)	1.32	1.60	0.041
	LP1 O(9)	$\sigma^*$ C(6)-H(7)	1.06	1.53	0.036
	LP2 O(9)	$\sigma^*$ C(6)-H(7)	7.61	1.15	0.084
	LP1 O(9)	$\sigma^*$ C(6)-H(8)	1.11	1.53	0.037
	LP2 O(9)	$\sigma^*$ C(6)-H(8)	7.49	1.15	0.083
	LP1 O(11)	$\sigma^*$ C(2)-C(3)	1.51	1.57	0.044
	LP2 O(11)	$\sigma^*$ C(2)-C(3)	7.44	1.22	0.085
	LP1 O(11)	$\sigma^*$ C(3)-H(4)	1.57	1.52	0.044
	LP2 O(11)	$\sigma^*$ C(3)-H(4)	7.65	1.16	0.084
	LP1 O(11)	$\sigma^*$ C(3)-H(5)	2.50	1.52	0.055
	LP2 O(11)	$\sigma^*$ C(1)-C(2)	0.90	0.83	0.024



BYDE



LP1	O(9)	$\sigma^*C(1)-C(6)$	1.32	1.60	0.041
LP1	O(9)	$\sigma^*C(6)-H(7)$	1.09	1.53	0.037
LP2	O(9)	$\sigma^*C(6)-H(7)$	7.62	1.15	0.084
LP1	O(9)	$\sigma^*C(6)-H(8)$	1.11	1.53	0.037
LP2	O(9)	$\sigma^*C(6)-H(8)$	7.58	1.15	0.084
LP1	O(11)	$\sigma^*C(3)-H(5)$	1.43	1.51	0.042
LP2	O(11)	$\sigma^*C(3)-H(5)$	7.90	1.16	0.086
LP1	O(11)	$\sigma^*C(3)-H(4)$	2.53	1.53	0.055
LP1	O(11)	$\sigma^*C(2)-C(3)$	1.65	1.58	0.046
LP2	O(11)	$\sigma^*C(2)-C(3)$	7.18	1.22	0.084
LP2	O(11)	$\sigma^*C(1)-C(2)$	0.57	0.83	0.022
LP2	O(11)	$\sigma^*C(1)-C(2)$	0.73	0.83	0.084

**Table 5:** Change in linearity of acetylene plane

Conformers	$\Delta(\Delta_{3,2,1})$	$\Delta(\Delta_{6,1,2})$	Change linearity(%)	in Change linearity(%)	in
BYDA-W	8	7	4.49	3.95	
BYDD-W	3	5	1.69	0.95	
BYDE-W	5	5	2.79	1.56	
BYDF-W	5	5	2.79	1.56	
BYDF-W'	-3	2	1.72	1.15	